

## Genome-wide analysis of brain age identifies 25 associated loci and unveils relationships with mental and physical health

Philippe Jawinski,<sup>1,2</sup> Helena Forstbach,<sup>1</sup> Holger Kirsten,<sup>2,3</sup> Frauke Beyer,<sup>4</sup> Arno Villringer,<sup>4</sup>  
A. Veronica Witte,<sup>4</sup> Markus Scholz,<sup>2,3</sup> Stephan Ripke,<sup>5,6</sup> Sebastian Markt<sup>1</sup>

<sup>1</sup> Department of Psychology, Humboldt-University Berlin, Berlin, Germany

<sup>2</sup> LIFE – Leipzig Research Center for Civilization Diseases, Leipzig University, Germany

<sup>3</sup> Institute for Medical Informatics, Statistics and Epidemiology, Leipzig University, Germany

<sup>4</sup> Cognitive Neurology, University of Leipzig Medical Center & Department of Neurology, Max Planck Institute for Human Cognitive and Brain Sciences, Leipzig, Germany

<sup>5</sup> Stanley Center for Psychiatric Research, Broad Institute of the Massachusetts Institute of Technology and Harvard University, Cambridge, Massachusetts, USA

<sup>6</sup> Department of Psychiatry and Psychotherapy, Charité - Universitätsmedizin, Berlin, Germany

### Abstract

Neuroimaging and machine learning are opening up new opportunities in studying biological aging mechanisms. In this field, ‘brain age gap’ has emerged as promising MRI-based biomarker quantifying the deviation between an individual’s biological and chronological age of the brain – an indicator of accelerated/decelerated aging. Here, we investigated the genetic architecture of brain age gap and its relationships with over 1,000 health traits. Genome-wide analyses in 32,634 UK Biobank individuals unveiled a 30% SNP-based heritability and highlighted 25 associated loci. Of these, 23 showed sign-consistency and 16 replicated in another 7,259 individuals. The leading locus encompasses *MAPT*, encoding the tau protein central to Alzheimer’s disease. Genetic correlations revealed relationships with various mental health (depression), physical health (diabetes), and socioeconomic variables (education). Mendelian Randomization indicated a causal role of enhanced blood pressure on accelerated brain aging. This work refines our understanding of genetically modulated brain aging and its implications for human health.

Keywords: aging, genetics, machine learning, mental health, MRI

### Corresponding author

Philippe Jawinski, Dr. rer. nat.

Department of Psychology, Humboldt-Universität zu Berlin

Unter den Linden 6, 01199 Berlin, Germany

Phone: +49 30 2093-9391

Email: [philippe.jawinski@hu-berlin.de](mailto:philippe.jawinski@hu-berlin.de)

## 1 Main

2 Aging is an intricate biological phenomenon inherent to most living organisms.<sup>1-3</sup> With extended  
3 human lifespans and the rapid pace of global demographic aging, age-related disabilities  
4 including neurodegenerative disorders such as dementia are on the rise.<sup>4</sup> Understanding the  
5 biological mechanisms of aging is thus an urgent priority for health and social systems, to sustain  
6 longer lives with reduced periods of disability.

7 The use of neuroimaging methods in conjunction with machine learning has become a  
8 promising avenue in biomedical research to capture an individual's biological age, with particular  
9 emphasis put on 'brain age'.<sup>5,6</sup> Brain age is typically assessed by training an age prediction model  
10 on in-vivo MRI data from a normative lifespan sample. This model is then applied to MRI data  
11 of unseen individuals to predict their age. The discrepancy between an individual's brain-  
12 predicted and chronological age is termed 'brain age gap' (BAG), and is used to draw inferences  
13 on typical and atypical aging trajectories.<sup>6,7</sup>

14 A positive BAG (interpreted as accelerated aging) has been linked to reduced mental and  
15 physical fitness,<sup>5</sup> including weaker grip strength, higher blood pressure, diabetes, adverse  
16 drinking and smoking behavior, poorer cognitive abilities, and depressive symptoms.<sup>8-13</sup>  
17 Enhanced BAG is also evident in neurological and psychiatric disorders such as Alzheimer's  
18 disease, schizophrenia, and bipolar disorder.<sup>14,15</sup> While previous genetic studies suggest that BAG  
19 exhibits a substantial heritable component, only few studies have identified specific genetic  
20 variants that contribute to BAG.<sup>15-21</sup> To refine the genetic architecture of BAG and identify  
21 potential therapeutic targets for healthy aging, further research is imperative.

22 In this report, we present what is to our knowledge the largest genome-wide association  
23 study (GWAS) of BAG to date. We discover novel loci in a sample of 32,634 individuals of  
24 white-British ancestry, and replicate our findings in a cross-ancestry sample of 7,259 individuals.  
25 This constitutes a 34% increase in sample size (about 10,000 more) compared to the most recent  
26 study<sup>20</sup> First, we prioritize genes using complementary fine-mapping, annotation, and co-  
27 localization strategies that integrate information from multiple omics resources. Second, we  
28 replicate variant effects and calculate polygenic scores to estimate the present yield in variance  
29 explanation. Third, we compute genetic correlations with over 1,000 health traits. Fourth, we  
30 use Mendelian Randomization to test a potential causal role of several risk factors in BAG.  
31 Finally, we examine the degree of polygenicity and project discoveries to forthcoming studies.  
32 By these efforts, we unravel new biological mechanisms behind BAG, such as binding of small  
33 GTPases, i.e., evolutionary conserved proteins that act as biological timers of cellular processes.

## 34 Results

35 Our brain age estimation workflow adhered to a well-established approach that utilizes the  
36 CAT12 voxel-based morphometry pipeline and has been validated extensively over the past  
37 years.<sup>5,22</sup> We used T1-weighted anatomical MRI scans and machine learning in a cross-validation  
38 manner to estimate brain age in a discovery sample of 32,634 white-British ancestry individuals  
39 of the UK Biobank (UKB) cohort (age range: 45-82 years).<sup>23</sup> Since brain aging has been  
40 demonstrated to encompass biologically distinct modes of change, we performed tissue-specific  
41 analyses on grey and white matter segmentations to increase the yield of biologically meaningful  
42 markers.<sup>18</sup> Machine learning was carried out using complementary algorithms: the sparse  
43 Bayesian relevance vector machine,<sup>24</sup> and the extreme gradient boosting technique (XGBoost)  
44 applied with both a tree and linear booster.<sup>25</sup> Trained models were stacked within and across  
45 tissue classes to enhance prediction accuracy. This revealed three brain-predicted age estimates  
46 per subject, representing the age prediction for grey matter, white matter, and combined grey  
47 and white matter.

**Table 1** Prediction accuracies of the stacked age estimation models stratified by tissue class

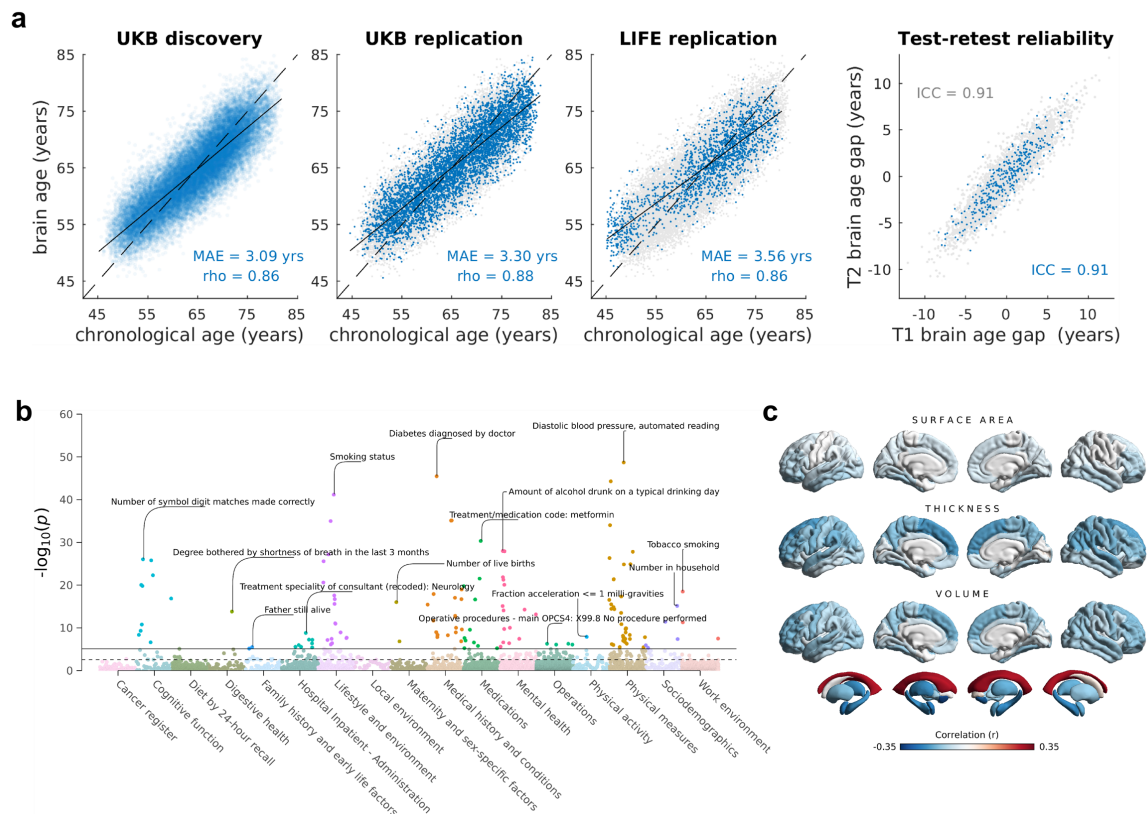
	UKB discovery ( $n = 32,634$ ; 45-82 years)			UKB replication ( $n = 5,427$ ; 44-83 years)			LIFE replication ( $n = 1,833$ ; 45-80 years)	
	$r$	MAE	ICC <sub>BAG</sub>	$r$	MAE	ICC <sub>BAG</sub>	$r$	MAE
Grey matter	.827	3.372	.898	.851	3.631	.893	.828	3.990
White matter	.835	3.307	.919	.859	3.562	.911	.829	3.979
Grey and white matter	.857	3.089	.914	.879	3.299	.909	.862	3.557

Note: Imaging data of the UKB discovery sample was released until January 2020 (release v1.7), while data of the UKB replication sample was released until September 2022 (release v1.9).  $r$ : product-moment correlation between brain-predicted age (without bias correction) and chronological age; MAE: mean absolute error of brain-predicted vs. chronological age; ICC<sub>BAG</sub>: intraclass correlation coefficient between test and re-test assessment of brain age gap. Brain age gap was bias-corrected for age, age<sup>2</sup>, sex, scanner site, and total intracranial volume. ICCs are based on a subset of 3,625 subjects in the UKB discovery and 376 subjects in the UKB replication sample.

48

49 In the discovery sample, we observed excellent prediction accuracies of chronological age,  
50 with mean absolute errors (MAE) reaching MAE = 3.09 years and correlation coefficients  
51 attaining  $r = .86$  (Fig. 1a, Table 1; details in suppl. Figure A1 and suppl. Table B1). Model  
52 performances were similar in two replication samples: a cross-ancestry UKB sample ( $n = 5,427$ ;  
53 age range: 45-80 years), and a European ancestry sample drawn from the LIFE-Adult cohort  
54 ( $n = 1,833$ ; age range: 45-80 years).<sup>26,27</sup> Noteworthy, genetic association analyses were performed  
55 on brain age gap (BAG), i.e., the discrepancy between an individual's brain-predicted and  
56 chronological age. These estimates – regressed on sex, age, age<sup>2</sup>, scanner site, and total  
57 intracranial volume – showed excellent test-retest reliabilities, with intra class correlation  
58 coefficients (ICC C,1)<sup>28</sup> ranging from .89 to .92.

59 To validate our BAG estimates and examine phenotypic relationships with health-related  
60 traits, we conducted a cross-trait association analysis between BAG and 7,088 non-imaging-  
61 derived phenotypes using PHESANT.<sup>29</sup> A total of 210 associations reached the Bonferroni-  
62 adjusted level of significance ( $p < 7.1e-06$ ) for at least one of the three BAG traits (suppl.  
63 Fig. A2, suppl. Table B2). Fig. 1b shows the cross-trait association results for combined grey  
64 and white matter BAG.



65  
66 **Fig. 1** Prediction accuracies and phenotypic associations for combined grey and white matter BAG. (a) Blue dots in the first three plots (from left to right) show brain-predicted age estimates plotted against chronological age in the UKB  
67 discovery sample ( $n = 32,634$ ), UKB replication sample ( $n = 5,427$ ), and LIFE-Adult replication sample ( $n = 1,883$ ).  
68 To facilitate comparisons, results of the UKB discovery sample are also shown as grey dots in the background of the  
69 UKB replication and LIFE replication plots. At this stage, brain-predicted age estimates have not yet been bias-corrected  
70 for regression dilution as indicated by the linear regression line (solid) crossing the identity line (dashed). The fourth  
71 plot shows the test-retest reliabilities of brain age gap in a subset of the UKB discovery (grey dots,  $n = 3,625$ ) and UKB  
72 replication sample (blue dots,  $n = 376$ ). Brain age gap was bias-corrected for age, age<sup>2</sup>, sex, scanner site, and total  
73 intracranial volume. (b) Cross-trait association results between brain age gap and 7,088 UK Biobank phenotypes from  
74 different health domains (sex, age, age<sup>2</sup>, scanner site, total intracranial volume served as covariates). Horizontal lines  
75 indicate the Bonferroni-adjusted (solid) and FDR-adjusted (dashed) level of significance. The top associations per  
76 category have been annotated. (c) Surface plots showing the correlations between brain age gap and 220 FreeSurfer  
77 brain structure variables. Colors reflect the strength and direction of partial product-moment correlations (sex, age, age<sup>2</sup>,  
78 scanner site, total intracranial volume served as covariates). MAE: mean absolute error; rho: product-moment correlation  
79 coefficient. ICC: intraclass correlation coefficient (C,1).<sup>28</sup>  
80

81 The top associations for combined BAG (all  $p \leq 1.8e-12$ ) included ‘pack years of smoking’  
82 ( $r = 0.091$ ), ‘diastolic blood pressure, automated reading’ ( $r = 0.084$ ), ‘number of symbol digit  
83 matches made correctly’ ( $r = -0.082$ ), ‘diabetes diagnosed by doctor’ ( $r = 0.079$ ), ‘amount of

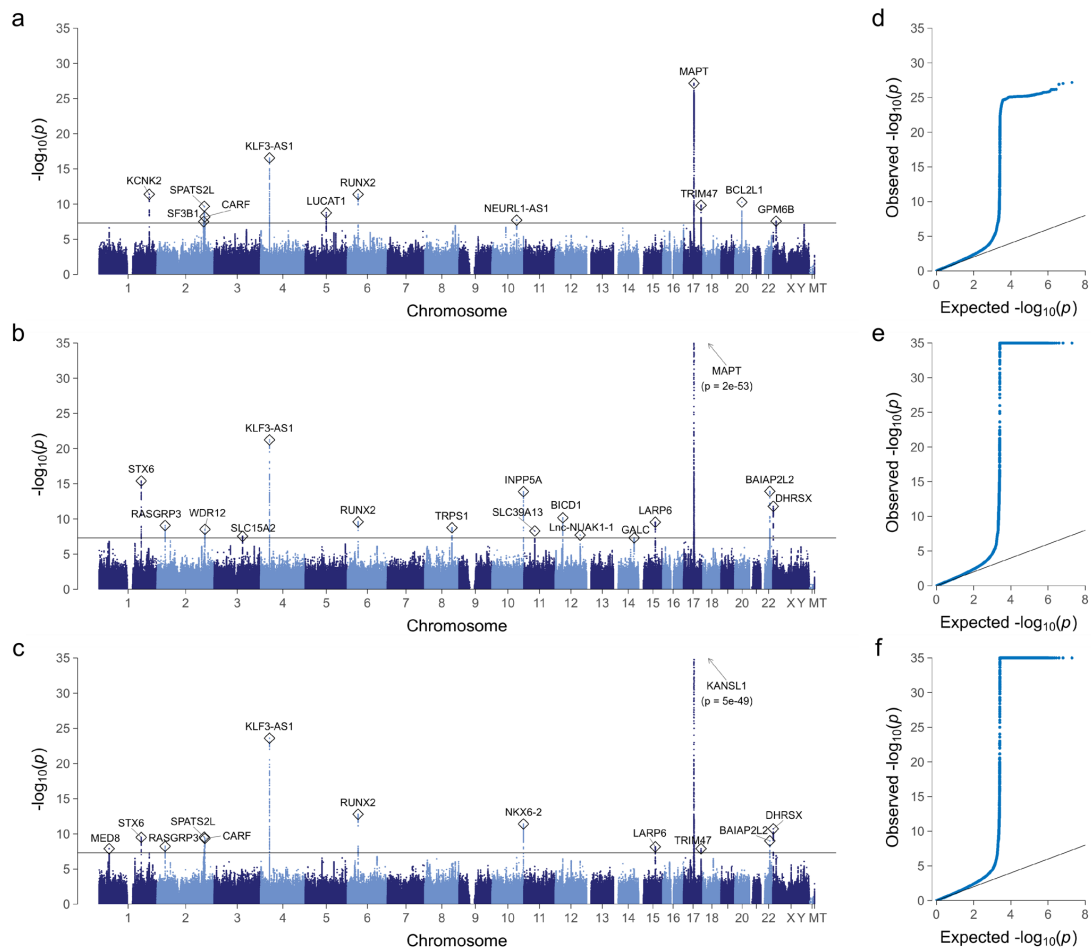
84 alcohol drunk on a typical drinking day' ( $r = 0.076$ ), and self-reported 'overall health rating'  
85 ( $r = 0.039$ ; higher ratings indicate poorer health).

86 To explore how BAG is reflected in individual brain regions, we calculated BAG  
87 associations with FreeSurfer<sup>30</sup> cortical surface measures and subcortical volumes (Fig. 1c, suppl.  
88 Fig. A3, suppl. Table B3). The strongest associations (all  $p \leq 4.9\text{e-}146$ ) were observed between  
89 BAG and volumes of the accumbentia ( $r = -0.31$ ), lateral ventricles ( $r = 0.29$ ), amygdalae  
90 ( $r = -0.25$ ), and hippocampi ( $r = -0.22$ ), as well as cortical thickness of the superior frontal  
91 ( $r = -0.16$ ) and superior temporal cortex ( $r = -0.14$ ). These results suggest that our models  
92 capture patterns of aging distributed throughout the brain, rather than being confined to specific  
93 brain areas. Moreover, results from cross-trait association analyses demonstrate relationships  
94 between BAG and multifaceted health traits, supporting the validity of BAG estimates.

### 95 **Discovery of 25 genomic loci**

96 To identify genetic loci associated with BAG, we conducted GWAS analyses based on 9,669,404  
97 Single Nucleotide Polymorphisms (SNPs) and insertion-deletions (INDELs) with  $\text{MAF} > 0.01$   
98 and  $\text{INFO} > 0.80$ . We modelled additive genetic effects, and used sex, age, age<sup>2</sup>, total intra-  
99 cranial volume, scanner site, type of genotyping array, and the first 20 genetic principal  
100 components as covariates. GWAS results for the three BAG traits are shown in Fig. 2.

101 LD score regression (LDSC) intercepts did not indicate a bias of test statistics due to  
102 reasons other than polygenicity, suggesting no confounding inflation due to population  
103 stratification (intercept range: 1.0075-1.0142; suppl. Table B4).<sup>31</sup> SNP-based heritability  
104 estimates derived from LDSC ranged between 26.2% (grey matter BAG) and 28.6% (white  
105 matter BAG). Estimates from GCTA-GREML<sup>32</sup> were slightly higher, suggesting SNP-based  
106 heritabilities of 28.9% for grey matter, 32.7% for white matter, and 32.3% for combined grey  
107 and white matter BAG ( $SE: 1.3\%$ ). The bivariate genetic correlation between grey and white  
108 matter BAG reached  $r_G = 0.703$  ( $SE = 0.018$ ), suggesting both shared and distinct genetic  
109 contributions. Stratified LDSC (suppl. Fig. A4, suppl. Table B5) revealed an enrichment of  
110 heritability (all  $FDR < 0.05$ ) in regions evolutionary conserved across mammals (fold enrichment  
111  $FE: 13.9$ ) and primates ( $FE: 12.7$ ). We also observed heritability enrichment in super enhancer  
112 ( $FE: 2.7$ ), and epigenetically modified H3K27ac ( $FE: 2.0$ ), H3K4me1 ( $FE: 1.9$ ), and H3K9ac  
113 regions ( $FE: 2.9$ ).



114

115 **Fig. 2** Manhattan plots (**a-c**) and quantile-quantile plots (**d-f**) showing the results of the discovery  
 116 genome-wide association analyses for the three brain age gap traits ( $N = 32,634$  UK Biobank individuals).  
 117 Manhattan plots show the  $p$ -values ( $-\log_{10}$  scale) of the tested genetic variations on the y-axis and base-  
 118 pair positions along the chromosomes on the x-axis. The solid horizontal line indicates the threshold of  
 119 genome-wide significance ( $p = 5E-8$ ). Index variations are highlighted by circles and were annotated with  
 120 those genes implicated by our gene prioritization analysis. Results of pseudoautosomal variations have been  
 121 added to chromosome 'X'. Quantile-quantile plots show the observed  $p$ -values from the association analysis  
 122 vs. the expected  $p$ -values under the null hypothesis of no effect ( $-\log_{10}$  scale). For illustrative reasons, the  
 123 y-axis has been truncated at  $p = 1e-35$ . **a,d** grey matter brain age gap; **b,e** white matter brain age gap;  
 124 **c,f** combined grey and white matter brain age gap.

125

126

127

128

129

130

131

132

To identify independent genome-wide significant associations, we conducted stepwise  
 conditional analyses using GCTA-COJO.<sup>32,33</sup> This resulted in 12 independent discoveries for grey  
 matter BAG, 16 for white matter BAG, and 13 for combined BAG (regional plots shown in  
 suppl. Fig. A5-12). Across the three BAG traits, the total count of independent discoveries was  
 25 (Table 1; suppl. Table B6), as determined through cross-trait LD clumping of index variations  
 ( $R^2 > 0.1$ ; 10 Mbp window-size). These 25 loci represent distinct genomic regions with a physical  
 distance larger than 2.5 Mbp. Among the 25 loci, 12 have previously been reported genome-wide  
 significant for BAG,<sup>15,17-20</sup> thus, 13 loci are novel findings.

**Table 2** Independent loci discovered through GWAS analyses of brain age gap in  $N = 32,634$  individuals

Locus	Cytoband	Chr	Position	ID	A1/A2	Freq	Beta (SE)	$p$	Prioritized Gene	Phenotype(s)	Repl.	Ref.
1	1p34.2	1	43,843,241	rs550778111	G/GT	0.414	0.149 (0.03)	1e-08	MED8	GWM	F	S
2	1q25.3	1	180,956,936	rs35306826	T/A	0.408	0.223 (0.03)	4e-16	STX6	WM,GWM	T	S
3	1q41	1	215,137,727	rs796226228	A/AT	0.375	-0.197 (0.03)	4e-12	KCNK2	GM	T	J
4	2p22.3	2	33,759,129	rs7605981	C/A	0.157	-0.226 (0.04)	9e-10	RASGRP3	WM,GWM	F	*
5	2q33.1	2	198,472,199	rs376899426	TAT/T	0.370	-0.157 (0.03)	3e-08	SF3B1	GM	F	*
6	2q33.1	2	201,147,317	rs377158217	CA/C	0.482	0.192 (0.03)	2e-10	SPATS2L	GM,GWM	F	*
7	2q33.2	2	203,664,929	rs76122535	G/C	0.135	-0.236 (0.04)	5e-10	CARF	GWM,WM,GM	T	*
8	3q13.33	3	121,643,447	rs34567530	AT/A	0.477	-0.150 (0.03)	3e-08	SLC15A2	WM	T	*
9	4p14	4	38,680,015	rs13132853	G/A	0.370	0.272 (0.03)	3e-24	KLF3-AS1	GWM,WM,GM	T	L,S
10	5q14.3	5	90,567,689	5:90567689	TTA/T	0.065	0.331 (0.06)	2e-09	LUCAT1	GM	T	*
11	6p21.1	6	45,428,508	rs35405209	TA/T	0.357	-0.203 (0.03)	2e-13	RUNX2	GWM,GM,WM	T	L,S,J
12	8q23.3	8	116,635,942	rs2721939	C/T	0.402	-0.165 (0.03)	2e-09	TRPS1	WM	T	*
13	10q24.33	10	105,459,116	rs4630220	A/G	0.285	-0.171 (0.03)	2e-08	NEURL1	GM	F	*
14	10q26.3	10	134,573,767	rs12258248	G/A	0.250	0.241 (0.03)	1e-14	NKX6-2	WM,GWM	T	L
15	11p11.2	11	47,606,865	rs12287076	G/C	0.294	-0.173 (0.03)	5e-09	SLC39A13	WM	F	*
16	12p11.21	12	32,526,829	rs6488048	C/T	0.348	-0.183 (0.03)	7e-11	BICD1	WM	F	*
17	12q23.3	12	106,476,805	rs12146713	C/T	0.095	0.257 (0.05)	2e-08	Lnc-NUAK1-1	WM	T	S
18	14q31.3	14	88,438,448	rs4904408	G/C	0.493	0.147 (0.03)	5e-08	GALC	WM	T	L
19	15q23	15	71,162,906	15:71162906	CA/C	0.397	-0.173 (0.03)	3e-10	LARP6	WM,GWM	F	S
20	17q21.31	17	44,276,431	rs111854640	TAG/T	0.227	0.494 (0.03)	2e-53	MAPT	WM,GWM,GM	T	N,L,S,J
21	17q25.1	17	73,872,969	rs3833085	AG/A	0.152	0.241 (0.04)	1e-10	TRIM47	GM,GWM	T	*
22	20q11.21	20	30,291,296	20:30291296	G/GT	0.249	-0.224 (0.03)	5e-11	FOXS1	GM	F	S
23	22q13.1	22	38,483,155	rs142739979	TTC/T	0.348	-0.222 (0.03)	1e-14	BAIAP2L2	WM,GWM	T	S
24	Xp22.2	X	13,893,318	rs5979992	G/C	0.326	0.132 (0.02)	3e-08	GEMIN8	GM	T	*
25	Xp22.33	XY	2,120,556	rs377113838	T/C	0.236	0.234 (0.03)	2e-12	DHRX	WM,GWM	T	*

Note: For each of the 25 loci, only the strongest variant-phenotype association is shown. Column 'Phenotype(s)' lists all brain age gap phenotypes with significant associations. The phenotype with the strongest association is mentioned first. For insertion/deletions, A1 and A2 alleles were truncated to three nucleotide bases.

Cytoband: cytogenetic band that contains the discovered locus; Chr: chromosome; Position: base pair position of index variation on chromosome; ID: identifier of index variation; A1: effect allele; A2: other allele; Freq: frequency of A1; Beta (SE): beta coefficient and standard error;  $p$ :  $p$ -value; Prioritized Gene: most relevant gene selected by our gene prioritization procedure; Phenotype(s): Traits for which a genome-wide significant association was found within that locus (grey matter GM, white matter WM, and combined grey and white matter brain age gap GWM), trait with strongest association is mentioned first; Rep.: indicator of locus replication status (one-tailed  $p < 0.05$ ), either true (T) or false (F); Ref.: previous studies that have reported this locus genome-wide significant, J: Jonsson et al. (2020), L: Leonardsen et al. (2023), N: Ning et al. (2019), S: Smith et al. (2020)

133 We observed the majority of index variations in intronic regions of protein-coding genes.  
 134 Consistently, ANNOVAR enrichment tests indicated that variants in high linkage disequilibrium  
 135 (LD) with our genome-wide significant variants were underrepresented in intergenic regions, and  
 136 over-represented in UTR3, UTR5, exonic, intronic, exonic non-coding RNA, and intronic non-  
 137 coding RNA regions (suppl. Fig. A13, suppl. Table B7).

138 **Fine-mapping and gene prioritization**

139 To shed light on the potential causal genes through which identified variants exert their effects  
140 on BAG, we used several fine-mapping, annotation, and co-localization strategies that integrate  
141 information from multiple omics resources. For each genome-wide significant locus, we a) inferred  
142 the number of distinct causal signals and constructed 95% credible sets of variants that likely  
143 include the causal variant using FINEMAP,<sup>34</sup> b) physically mapped credible variants to genes  
144 using ANNOVAR,<sup>35</sup> c) predicted transcript consequences of non-synonymous exonic credible  
145 variants and scored their deleteriousness using CADD,<sup>36</sup> DANN,<sup>37</sup> and REVEL,<sup>38</sup> d) mapped  
146 variants to genes through expression quantitative trait locus (eQTL) lookup in 49 GTEx v8  
147 tissues,<sup>39</sup> e) conducted summary-data-based Mendelian Randomization (SMR)<sup>40,41</sup> with RNA  
148 sequence data of 2,865 brain cortex samples<sup>42</sup> to test for mediation of variant effects through  
149 gene expression and splicing, and f) calculated polygenic priority scores (PoPS)<sup>43</sup> that  
150 incorporate data from single-cell RNA sequencing datasets, curated biological pathways, and  
151 protein-protein interaction (PPI) networks. Across all genes nominated by abovementioned  
152 strategies, we computed an integrative gene priority score and prioritized the most relevant gene  
153 (see methods). Figure 3 provides an overview of the analysis workflow. A locus-wise summary  
154 of all results is shown in suppl. Table B6 (details in suppl. Tables B7-B15).

155 For the 25 discovered loci, FINEMAP revealed a model-averaged number of  $k$  causal  
156 signals per locus ranging from 1.04 to 2.06 (median: 1.24), with the most probable  $k$  model  
157 suggesting 1 causal signal for 21 loci, and 2 causal signals for 4 loci (suppl. Table B6). This  
158 finding is largely consistent with conditional analysis results, suggesting 1 independent signal for  
159 each locus. The size of the 95% credible set of variants ranged between 4 and 2,514 (median:  
160 46), indicating a small pool of causal candidates for some loci and a putative complex linkage  
161 structure that hinders pinpointing causal variants for other loci. The estimated per-locus  
162 contribution to the phenotypic variance, i.e., the regional heritability, ranged between 0.09%  
163 and 0.70%.



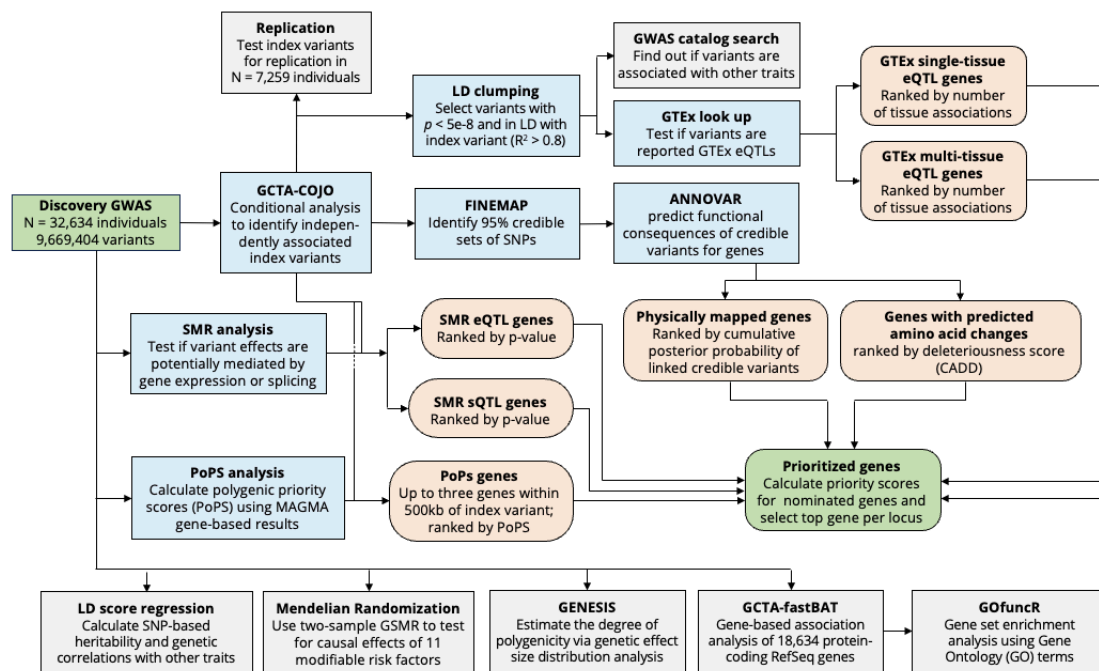


**Fig. 3** Overview of the post-GWAS analysis workflow including the gene prioritization procedure. Green boxes represent data input (discovery GWAS) and output (prioritized genes). Blue boxes represent analyses whose outcomes were used for gene nomination and subsequent prioritization. Apricot-colored boxes reflect gene nomination categories. Grey boxes reflect all other analyses carried out to refine the genetic architecture of brain age gap such as heritability and polygenicity analyses. Genes were prioritized by integrating data from multiple strategies such as functional annotation of credible variants, summary-data-based Mendelian Randomization (SMR), GTEx eQTL lookups, and Polygenic Priority Scores (PoPS).

We observed the strongest associations at locus 17q21.31 (rs111854640,  $p = 2.3E-53$ ), which tags a well-known 900kb inversion polymorphism.<sup>44,45</sup> This region is one out of three with alternate haplotype reference sequences included in genome assembly GRCh37 (UCSC haplotype sequence: chr17\_ctg5\_hap1). Consistent with the strong LD cluster in the inverted region,<sup>44</sup> we found this locus with by far the largest credible set of variants (2,514). We carried out an NHGRI-GWAS catalog search to identify pleiotropic effects with other complex traits.<sup>46</sup> This search revealed a large variety of locus-associated traits, including educational attainment,<sup>47</sup> depressed affect,<sup>48</sup> alcohol consumption,<sup>49</sup> sleep duration,<sup>50</sup> lung function,<sup>51</sup> male puberty timing,<sup>52</sup> age at onset of menarche,<sup>51</sup> and Alzheimer's disease.<sup>53</sup> The locus covers multiple genes, including *MAPT*, *STH*, *KANSL1*, and *CRHR1*. Several genome-wide significant variants in these genes are GTEx single-tissue and multi-tissue eQTLs (suppl. Tables B12-B13). SMR analyses implicated alterations in gene expression and splicing of *MAPT* and *KANSL1* as putative mechanisms that mediate variant effects on BAG (suppl. Tables B10-11). Additionally, we identified several exonic variants causing amino-acid changes in transcript sequences (suppl. Table B9). The highest CADD deleteriousness score was shown for rs176515149 (CADD score: 34), located in exon 6 of *MAPT*, with a GWAS  $p$ -value of 4.9e-52. This variant causes an arginine-to-tryptophan substitution at MAPT protein position 370. *MAPT* encodes the well-

190 known ‘tau protein’ implicated in Alzheimer’s and other neurodegenerative diseases.<sup>54</sup>  
191 Altogether, we prioritized *MAPT* as most plausible susceptibility gene for brain aging in this  
192 locus.

193 Three other loci were identified with a tractable number ( $\leq 10$ ) of likely causal variants.  
194 The first locus with 4 credible variants refers to an intergenic region at 1q41, 41 kb upstream of  
195 *KCNK2*, encoding Potassium channel subfamily K member 2. *KCNK2* is also prioritized by  
196 SMR, GTEx, and PoPS analyses. *KCNK2* has been implicated in neuroinflammation, blood-  
197 brain barrier dysfunction, and cerebral ischemia.<sup>55,56</sup> GWAS catalog matches suggest  
198 associations with cortical thickness,<sup>57</sup> surface area,<sup>58</sup> and sulcal opening.<sup>59</sup>

199 The second locus, again with 4 variants in the 95% credible set, refers to an intronic region  
200 of *NUAK1* at 12q23.3. Index variant rs12146713 is a multi-tissue eQTL of *Lnc-NUAK1-1*, i.e.,  
201 a long non-coding RNA gene expressed in brain cortex, cerebellum, and other tissues. GWAS  
202 catalog matches suggest further associations with cortical thickness,<sup>57</sup> surface area,<sup>58</sup> and  
203 subcortical volume.<sup>57</sup>

204 The third locus refers to exon 11 of *BAIAP2L2* at 22q13.1, with 9 variants in the 95%  
205 credible set. Index variant rs142739979 is a non-frameshift INDEL predicted to cause an insertion  
206 of threonine, proline, and methionine between *BAIAP2L2* protein sequence positions 411 and  
207 412. Additionally, this variant is a reported eQTL of nine genes, including *SLC16A8* linked to  
208 age-related macular degeneration,<sup>60</sup> and *TRIOBP*, whose protein isoforms have been implicated  
209 in neurite outgrowth, cell cycle progression, and motility of cancer cells.<sup>61</sup>

210 While above-mentioned loci have also been supported in previous studies, we here discover  
211 several novel loci that offer new insights into the biological path-mechanisms of brain aging. One  
212 of them refers to a UTR5-region of *TRPS1* at 8q23.3, with *TRPS1* also representing the  
213 prioritized gene. Previous studies have implicated variants in strong LD ( $R^2 > 0.8$ ) with the  
214 index variant in neuroticism,<sup>48</sup> type-2 diabetes,<sup>62</sup> and anthropometric measures.<sup>63</sup> *TRPS1* is a  
215 transcription factor that represses the expression of GATA-regulated genes in vertebrate  
216 development,<sup>64</sup> and has been implicated in a large variety of physiological processes including  
217 organ differentiation and tumorigenesis.<sup>65</sup>

218 Another novel discovery refers to an intronic region of *ICA1L* at 2q33.2, led by rs76122535  
219 ( $p = 4.6e-10$ ), with GTEx and SMR analysis indicating variant effects on expression and splicing  
220 of *ICA1L*, *CARF*, and *NBEAL1* in a variety of tissues. The highest priority score was attained  
221 by *CARF*, which is reportedly upregulated during stress-induced and oncogenic senescence, and  
222 its overexpression has been observed to cause premature senescence.<sup>66</sup>

223 Furthermore, we identified an X-chromosomal locus in an intron of *GPM6B*, led by  
224 rs597999 ( $p = 2.7e-08$ ), which is also a GTEx eQTL of *GPM6B*. The *GPM6B* protein has been

225 suggested to regulate serotonin uptake, is particularly expressed in brain tissue, and belongs to  
226 the proteolipid protein family involved in cell-to-cell communication.<sup>67</sup>

227 A final novel discovery to be mentioned refers to a variant near *DHRXSX*, tagged by  
228 rs377113838 ( $p = 1.6\text{e-}12$ ), which is a GTEx multi-tissue eQTL of the same gene, and lies in a  
229 pseudoautosomal region, i.e., a region with homologous sequences on chromosome X and Y.  
230 *DHRXSX* has been shown to play a crucial role in starvation-induced autophagy.<sup>68</sup>

231 As strongest known risk factor for Alzheimer's disease, we tested the  $\epsilon 4$  allele of the  
232 apolipoprotein E (*APOE*) gene, determined from haplotypes of rs429358 and rs7412, for BAG  
233 associations. The number of  $\epsilon 4$  alleles was indeed associated with higher BAG ( $p = 7.8\text{e-}06$ ),  
234 although not attaining genome-wide significance.

235 Altogether, by integrating information from several fine-mapping, functional annotation,  
236 and colocalization strategies we here prioritized several genes potentially involved in brain aging.  
237 These leads may stimulate novel testable hypotheses on the causes of biological aging.

### 238 **Replication of discovered variants**

239 Independent discoveries from the SNP-level analysis were tested for replication in a follow-up  
240 cross-ancestry meta-analysis of up to 7,259 individuals (suppl. Table B15, suppl. Fig. A14-A17).  
241 Replication analyses included index variations from the 25 genome-wide significant loci, and  
242 index variations from another 45 suggestive loci (conditional  $p$ -values ranging from  $1.0\text{e-}06$  to  
243  $5.0\text{e-}08$ ). The degree of consistency between discovery and replication results was highly unlikely  
244 to occur by chance (suppl. Fig. A18). Of the 25 discoveries, 23 showed consistent effect directions  
245 (binomial test:  $p = 9.7\text{e-}06$ ) and 16 replicated at  $p < 0.05$  (one-tailed nominal significance;  
246 binomial test:  $p = 2.0\text{e-}15$ ). This finding aligns closely with the outcomes predicted by statistical  
247 power analyses, with 16.51 out of 25 loci expected to attain one-tailed nominal significance in  
248 replication analyses. All replicated loci are highlighted in Table 2 (column 'Rep.'). Novel  
249 replicated loci included 2q33.2 (rs76122535 near *CARF*), 3q13.33 (rs34567530 in *SLC15A2*),  
250 5q14.3 (5:90567689\_TTA\_T near *LUCAT1*), 8q23.3 (rs2721939 in *TRPS1*), 17q25.1 (rs3833085  
251 in *TRIM47*), Xp22.2 (rs5979992 in *GPM6B*), and Xp22.33 (rs377113838 near *DHRXSX*,  
252 pseudoautosomal).

253 Among the additional 45 suggestive variants, we found 35 with consistent effect directions  
254 (binomial test:  $p = 1.2\text{e-}04$ ) and 14 attaining one-tailed nominal significance in replication  
255 analyses (binomial test:  $p = 2.3\text{e-}08$ ). Moreover, we found polygenic scores (PGS) with variance  
256 explanations of 2.1% for grey matter, 2.8% for white matter, and 2.5% for combined BAG (all  
257  $p \leq 5.1\text{e-}22$ ; suppl. Table B17). Proportions of explained variance were lower when considering  
258 only genome-wide significant discoveries (0.8-1.3%; all  $p \leq 1.5\text{e-}09$ ). In sum, replication results

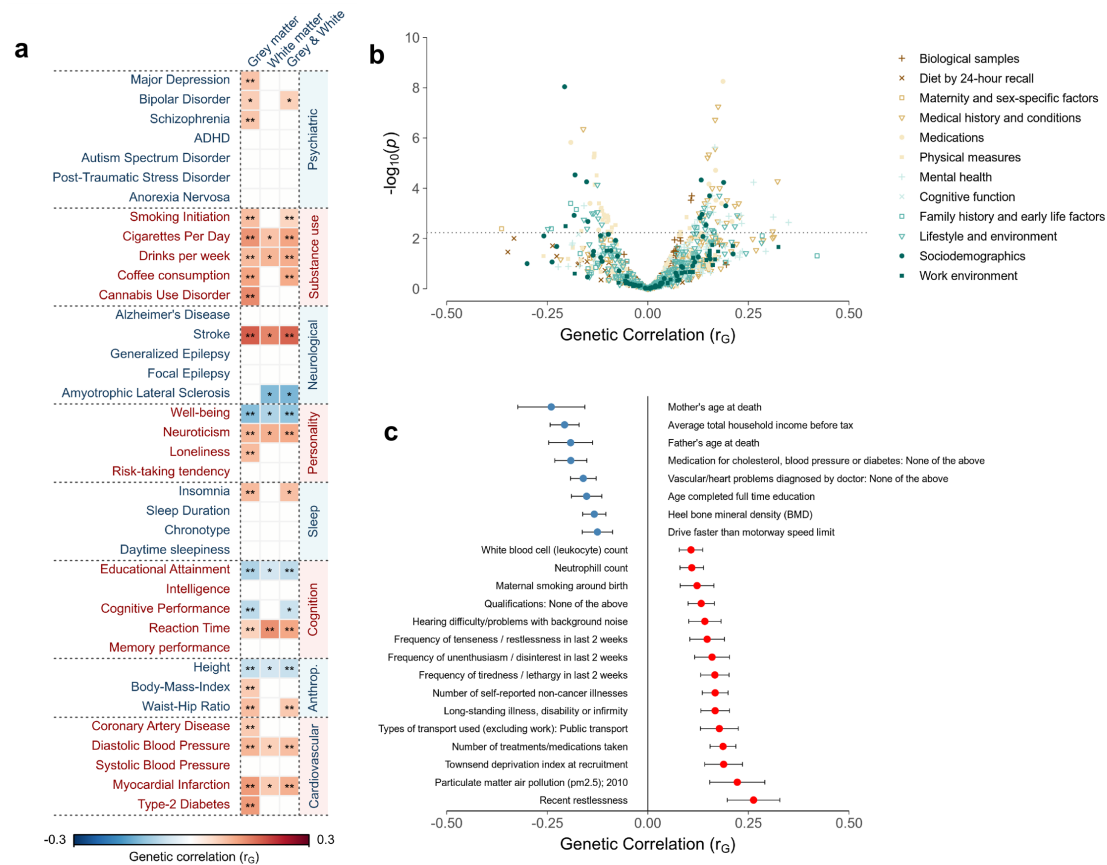
259 provide strong support for true associations among the discovered loci and point towards  
260 additional contributions at sub-threshold significance levels.

### 261 **Gene-based analysis**

262 We investigated the potential impact of 18,643 protein-coding genes using GCTA-fastBAT.<sup>69</sup>  
263 Gene-based analyses aggregate information from multiple variants within the same genomic  
264 region, resulting in a reduced multiple-testing burden compared to variant-based analyses. Gene-  
265 based analyses revealed 188, 327, and 295 genes significantly associated (FDR < 0.05) with grey  
266 matter, white matter, and combined grey and white matter BAG, respectively. To identify  
267 independent associated loci, we conducted a *p*-value informed clumping procedure of genes  
268 located in a physical distance of 3,000 kbp. This resulted in 69, 114, and 97 distinct loci,  
269 respectively, of which 151 were unique across the three phenotypes (suppl. Fig. A19, suppl. Table  
270 B18). Again, the strongest signal was observed at 17q21.31 covering *MAPT*. Significant genes  
271 also included *APOE* (encoding apolipoprotein E), i.e., the gene with the strongest known impact  
272 on late-onset Alzheimer's disease.<sup>70</sup> In total, gene-based analyses provide evidence for an  
273 extended set of genomic loci involved in human brain aging.

### 274 **Pathway analysis**

275 To gain further insights into the biological mechanisms underlying brain aging, we used gene-  
276 based results to test for an enrichment of Gene Ontology (GO) terms, i.e., sets of genes known  
277 to serve a common biological function.<sup>71</sup> Gene set enrichment analyses (GSEA) were conducted  
278 using GOfuncR.<sup>72</sup> GSEA revealed nine significant GO terms (suppl. Table B19) after refinement  
279 of hierarchical dependencies. Analyses provided indications for a role of the immune system in  
280 brain aging, with significant results obtained for 'MHC protein complex' (GO:0042611) and  
281 'peptide antigen binding' (GO:0042605). Results also implicated 'small GTPase binding'  
282 (GO:00312671) as potential mechanism in brain aging. Small GTPases are a superfamily of  
283 evolutionary conserved proteins that act as biological timers (binary on/off switches) of many  
284 essential cellular processes.<sup>73,74</sup> These processes include cell differentiation, proliferation, and  
285 signal transduction.<sup>75</sup> Several small GTPase proteins have been implicated in premature  
286 senescence.<sup>76-78</sup>



287

288 **Fig. 4** Results from the genetic correlation analyses between brain age gap and 1,027 other complex  
289 phenotypes. **(a)** Genetic correlation matrix between brain age gap (columns) and 38 selected phenotypes  
290 from different health domains (rows). \*  $p < 0.05$  (nominal significance) \*\* FDR  $< 0.05$  (level of significance  
291 after multiple testing-correction) **(b)** Volcano plot showing the magnitude (x-axis) and significance (y-axis)  
292 of genetic correlations between grey matter brain age gap and 989 traits examined by Neale and colleagues.  
293 The dashed horizontal line indicates the FDR-adjusted level of significance. **(c)** Forest plot showing the  
294 genetic correlation coefficients and standard errors for a subset of 23 exemplary traits that showed  
295 significant genetic correlations with grey matter brain age gap.

## 296 Genetic correlations with other complex traits

297 To examine a potential shared genetic basis with other complex traits, we applied bivariate LD  
298 score regression<sup>31,79</sup> to GWAS summary statistics and calculated genetic correlations with 38  
299 frequently employed traits from different mental and physical health domains (suppl. Table  
300 B20).<sup>80-82</sup> We also calculated genetic correlations with 989 heritable traits from a large set of  
301 GWAS summary statistics (Zenodo: <https://doi.org/10.5281/zenodo.7186871>). In total, we  
302 observed 22 out of 38 selected traits to significantly correlate (FDR  $< 0.05$ ) with at least one of  
303 the three BAG variables (Fig. 4a, suppl. Table B21). Grey matter BAG showed the highest  
304 number of significant associations (22), relative to white matter (1) and combined grey and  
305 white matter BAG (13). A similar pattern was observed for the 989 traits, where we observed  
306 121, 2, and 36 significant associations for the three BAG traits, respectively (Fig. 4b and 4c,  
307 suppl. Table B22).

308 Among the 38 selected traits, we found significant associations between grey matter BAG  
309 and psychiatric (e.g., Major Depression:  $r_G = 0.085$ ), substance use (cigarettes per day:  
310  $r_G = 0.134$ ), neurological (stroke:  $r_G = 0.182$ ), personality (neuroticism:  $r_G = 0.100$ ), sleep-  
311 related (insomnia:  $r_G = 0.096$ ), cognition-related (educational attainment:  $r_G = -.091$ ),  
312 anthropometric (body-mass-index:  $r_G = 0.075$ ), as well as cardiovascular and metabolic  
313 syndrome traits (type-2 diabetes:  $r_G = 0.127$ ).

314 Among the 989 heritable traits, we found evidence for genetic correlations with ‘mother’s  
315 age at death’ ( $r_G = -0.240$ ) and ‘father’s age at death’ ( $r_G = -0.192$ ), suggesting that higher  
316 BAG is associated with shorter familial life expectancy. Other significant associations referred  
317 to socioeconomic variables (e.g., ‘average total household income before tax’:  $r_G = -0.207$ ),  
318 mental health variables (‘frequency of tiredness/lethargy in last 2 weeks’:  $r_G = 0.167$ ), medical  
319 conditions (‘Vascular/heart problems diagnosed by doctor: High blood pressure’:  $r_G = 0.149$ ),  
320 medication intake (e.g. ‘medication for cholesterol, blood pressure or diabetes: None’:  
321  $r_G = -0.191$ ), early life factors (‘maternal smoking around birth’:  $r_G = 0.122$ ), among others  
322 (suppl. Table B22). These results suggest a shared genetic basis between BAG and a broad range  
323 of health-related variables.

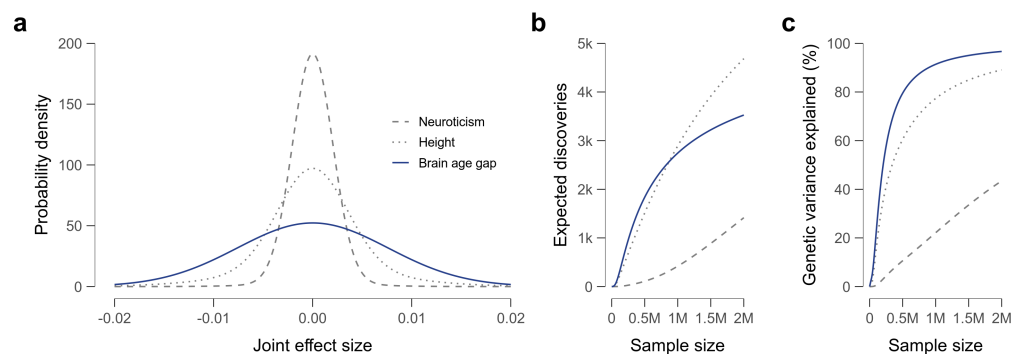
### 324 **Causal associations**

325 We used two-sample generalized summary-data-based Mendelian Randomization (GSMR)<sup>83</sup> to  
326 investigate potential causal effects of 12 modifiable risk/resilience factors on BAG. The  
327 risk/reliance factors were BMI, waist-hip-ratio adjusted for BMI, low-density lipoprotein  
328 cholesterol (LDL-c), high-density lipoprotein cholesterol (HDL-c), triglycerides, systolic blood  
329 pressure, diastolic blood pressure, pulse pressure, type-2-diabetes, coronary artery disease,  
330 schizophrenia, and years of education. Our analyses revealed significant effects of diastolic blood  
331 pressure on all three BAG traits (combined BAG:  $\beta_{xz} = 0.610$ ,  $p = 1.4e-08$ ), as well as systolic  
332 blood pressure on grey matter ( $\beta_{xz} = 0.443$ ,  $p = 5.8e-05$ ) and combined BAG ( $\beta_{xz} = 0.326$ ,  
333  $p = 0.002$ ).<sup>84</sup> Results suggest that one standard deviation increase in blood pressure causally  
334 contributes to an about half-year increase in BAG (suppl. Table B24, suppl. Fig. A20-22).

### 335 **Degree of polygenicity and projection of discoveries to future GWAS**

336 To quantify the degree of polygenicity and predict the number of discoveries in forthcoming  
337 GWAS, we used GENESIS<sup>85</sup> and estimated the number of underlying susceptibility variants and  
338 their effect sizes. We considered ‘height’ and ‘neuroticism’ as benchmark traits due to their  
339 different degrees of polygenicity.<sup>86-89</sup> For the three BAG traits, the number of susceptibility  
340 variants was consistently estimated at 5.7k (SE 1.7k; suppl. Table B25). By comparison, this  
341 number was estimated at 12.6k (SE 1.3k) for height and 16.2k (SE 1.2k) for neuroticism. The

342 distributions of variant effect sizes (Fig. 5a) revealed that BAG exhibits a greater proportion of  
343 contributing variants with large effect sizes when compared to neuroticism and standing height.



344

345 **Fig. 5** Results of the genetic effect size distribution analysis for combined grey and white matter brain  
346 age gap. Neuroticism and standing height serve as reference traits. (a) Effect-size distributions of underlying  
347 susceptibility variants. Wider tails indicate a greater proportion of susceptibility variants with large effect  
348 sizes. (b) Expected number of discoveries as a function of sample size. (c) Expected proportion of genetic  
349 variance explained by genome-wide significant discoveries as a function of sample size.

350 Moreover, the number of discoveries for BAG was predicted to show rapid increases with rising  
351 sample sizes (Fig. 5b). Fig. 5c shows that about 500k subjects are required to explain 80% of  
352 the SNP-based heritability for BAG from genome-wide significant discoveries. This number  
353 aggregates to about 1M for height and 6M for neuroticism. Together, these results suggest a  
354 relatively low degree of polygenicity for BAG when compared to other complex traits.

## 355 Discussion

356 We here leveraged genomic and neuroimaging methods to demonstrate the significance of brain  
357 age gap (BAG) as a putative biomarker of aging and its prospective utility in identifying  
358 therapeutic targets. Machine learning and MRI quantified brain age with excellent measurement  
359 properties, capturing distributed patterns of aging across the brain. Cross-trait association  
360 analyses established robust associations with various health traits, highlighting the potential  
361 clinical relevance of BAG. We showed that BAG is under substantial genetic control, with about  
362 30% of the phenotypic variance attributable to common genetic variation. We identified 25  
363 independent genome-wide significant loci, of which 13 loci are novel. The observed genomic  
364 signals unveiled several enriched biological pathways, e.g., immune-system-related processes as  
365 well as the binding of small GTPases, prompting further mechanistic exploration. Using genetic  
366 correlations, we characterized the common genetic basis between BAG and other complex traits,  
367 including psychiatric, neurological, cognitive, personality, substance use, sleep-related, as well as  
368 cardiovascular and metabolic syndrome traits. Through Mendelian Randomization, we  
369 established evidence for a causative role of enhanced blood pressure in accelerated brain aging.

370 Finally, we find BAG with a relatively low degree of polygenicity, and we anticipate this will  
371 facilitate further variant discoveries in the near future.

372 Brain aging is not a uniform process; rather, it encompasses diverse aspects of structural  
373 and functional change. Studying different aspects of brain aging has been advocated to increase  
374 the yield of biologically meaningful insights.<sup>18</sup> We calculated separate BAG for the brain tissue  
375 classes grey matter and white matter, in addition to a composite measure. For both tissues, we  
376 found remarkably consistent age prediction accuracies, along with comparable test-retest  
377 reliabilities and heritabilities. The genetic correlation between grey and white matter BAG,  
378 however, settled at  $r_G = 0.70$  (SE 0.018), suggesting both shared and segregated biological  
379 underpinnings. While grey matter and white matter BAG exhibit comparable SNP-based  
380 heritabilities (0.289 vs. 0.327; SE: 0.013), grey matter BAG showed a noticeably higher number  
381 of significant phenotypic and genetic associations, which may imply greater relevance for several  
382 health dimensions. This subject warrants more in-depth exploration in future research.

383 We confirmed the previously reported inversion locus at 17q21.31 as strongest known  
384 genetic contributor to BAG,<sup>17,19–21</sup> explaining 0.3% of the variance in grey matter and 0.7% in  
385 white matter BAG. The most likely causative gene in this locus, *MAPT*, encodes the well-known  
386 ‘tau’ protein associated with Alzheimer’s disease. Genomic analyses also unveiled a role of  
387 Alzheimer’s risk gene *APOE* and other apolipoprotein genes. With both tau- and apolipoprotein  
388 alterations, our results implicate two hallmarks of Alzheimer’s in accelerated brain aging. This  
389 aligns with the demonstrated capability of BGA to forecast Alzheimer's disease.<sup>90</sup>

390 Two prior studies on BAG have attempted to replicate variant discoveries, albeit with  
391 limited success.<sup>17,20</sup> Here we observed a high degree of consistency between discovery and  
392 replication results, with 23 out of 25 loci showing consistent effect directions, and 16 loci  
393 attaining nominal significance in replication analyses. Notably, polygenic scores accounted for  
394 about 2-3% of the phenotypic variance, a remarkable proportion when compared to traits such  
395 as intelligence and major depressive disorder, which necessitated considerably larger discovery  
396 samples to attain similar prediction accuracies.<sup>82,91</sup>

397 The current study has several limitations. First, the employed gene prioritization  
398 techniques face challenges in pinpointing causal genes,<sup>43</sup> particularly for loci characterized by  
399 high gene density and complex linkage structures. Second, BAG has been estimated from cross-  
400 sectional data, which is typically interpreted as accelerated or decelerated aging. However, an  
401 alternative interpretation posits BAG as stable individual differences that emerge at an  
402 ontogenetically early period and are carried into old age.<sup>92</sup> Third, statistical power analyses  
403 revealed an expected number of 16 successful replications (out of 25), indicating a need for higher  
404 replication sample sizes. Fourth, polygenic overlap between different traits was estimated using



405 genetic correlations. Yet, this technique does not capture fractions of genetic variants shared  
406 between two traits irrespective of variant effect directions. Other bioinformatic tools such as  
407 MiXeR may be used in future studies to quantify genetic overlap by considering mixtures of  
408 variant effects.<sup>93</sup> Fourth, polygenicity models are known to classify variants with very low effect  
409 sizes as null, resulting in a likely underestimation of BAG polygenicity estimates.

410 In conclusion, the present study refines the genetic architecture of brain age gap and its  
411 relationships to other traits. We added 13 new variants to the catalogue of existing BAG  
412 associations and assigned plausible candidates to these loci such as TRPS1 implicated in various  
413 pathological processes, GPM6b involved in cell-to-cell communication, and CARF linked to  
414 premature senescence. This will facilitate further work on path-mechanisms of BAG and  
415 potential therapy targets.

## 416 **Acknowledgments**

417 This research has been conducted using the UK Biobank Resource under Application Number  
418 423032. This publication was supported by LIFE – Leipzig Research Centre for Civilization  
419 Diseases, University of Leipzig. LIFE was funded by means of the European Social Fund and  
420 the Free State of Saxony. We thank the ICBP consortium for providing summary statistics.

## 421 **Conflict of Interest**

422 The authors declare no conflict of interest.

## 423 **Data availability**

424 The individual-level data incorporated in this work have been obtained from the UK Biobank  
425 resource (<https://www.ukbiobank.ac.uk/>). GWAS summary statistics for BAG will be made  
426 available at Zenodo (<https://zenodo.org/>) upon publication of this article.

## 427 **Code availability**

428 All scripts used in this work are available on GitHub  
429 ([https://github.com/pjawinski/ukb\\_brainage](https://github.com/pjawinski/ukb_brainage))

## 430 **Supplementary Material**

431 Supplementary information is available at bioRxiv online.

## 432 **References**

433 1. Kirkwood, T. B. L. Understanding the odd science of aging. *Cell* vol. 120 437–447

- 434 (2005).
- 435 2. da Silva, R., Conde, D. A., Baudisch, A. & Colchero, F. Slow and negligible senescence  
436 among testudines challenges evolutionary theories of senescence. *Science (80-. )*. **376**,  
437 1466–1470 (2022).
- 438 3. Finch, C. E. & Austad, S. N. History and prospects: symposium on organisms with  
439 slow aging. *Exp. Gerontol.* **36**, 593–597 (2001).
- 440 4. Vos, T. *et al.* Years lived with disability (YLDs) for 1160 sequelae of 289 diseases and  
441 injuries 1990&#x2013;2010: a systematic analysis for the Global Burden of Disease  
442 Study 2010. *Lancet* **380**, 2163–2196 (2012).
- 443 5. Franke, K. & Gaser, C. 10 years of BrainAGE as an neuroimaging biomarker of brain  
444 aging: What insights did we gain? *Front. Neurol.* **10**, 789 (2019).
- 445 6. Cole, J. H., Marioni, R. E., Harris, S. E. & Deary, I. J. Brain age and other bodily  
446 ‘ages’: implications for neuropsychiatry. *Mol. Psychiatry* **24**, 266–281 (2019).
- 447 7. Liem, F. *et al.* Predicting brain-age from multimodal imaging data captures cognitive  
448 impairment. *Neuroimage* **148**, 179–188 (2017).
- 449 8. Franke, K., Gaser, C., Manor, B. & Novak, V. Advanced BrainAGE in older adults  
450 with type 2 diabetes mellitus. *Front. Aging Neurosci.* **5**, 90 (2013).
- 451 9. Franke, K., Ristow, M. & Gaser, C. Gender-specific impact of personal health  
452 parameters on individual brain aging in cognitively unimpaired elderly subjects. *Front.*  
453 *Aging Neurosci.* **6**, (2014).
- 454 10. Steffener, J. *et al.* Differences between chronological and brain age are related to  
455 education and self-reported physical activity. *Neurobiol. Aging* **40**, (2016).
- 456 11. Richard, G. *et al.* Assessing distinct patterns of cognitive aging using tissue-specific  
457 brain age prediction based on diffusion tensor imaging and brain morphometry. *PeerJ*  
458 **2018**, (2018).
- 459 12. Cole, J. H. *et al.* Brain age predicts mortality. *Mol. Psychiatry* **23**, 1385–1392 (2018).
- 460 13. Jawinski, P. *et al.* Linking Brain Age Gap to Mental and Physical Health in the Berlin  
461 Aging Study II. *Front. Aging Neurosci.* **14**, (2022).
- 462 14. Shahab, S. *et al.* Brain structure, cognition, and brain age in schizophrenia, bipolar  
463 disorder, and healthy controls. *Neuropsychopharmacol. Off. Publ. Am. Coll.*  
464 *Neuropsychopharmacol.* **44**, 898–906 (2019).
- 465 15. Kaufmann, T. *et al.* Common brain disorders are associated with heritable patterns of  
466 apparent aging of the brain. *Nat. Neurosci.* **22**, 1617–1623 (2019).
- 467 16. Cole, J. H. *et al.* Predicting brain age with deep learning from raw imaging data results  
468 in a reliable and heritable biomarker. *Neuroimage* **163**, 115–124 (2017).
- 469 17. Jonsson, B. A. *et al.* Brain age prediction using deep learning uncovers associated  
470 sequence variants. *Nat. Commun.* **10**, 5409 (2019).
- 471 18. Smith, S. M. *et al.* Brain aging comprises many modes of structural and functional  
472 change with distinct genetic and biophysical associations. *Elife* **9**, e52677 (2020).
- 473 19. Ning, K. *et al.* Improving brain age estimates with deep learning leads to identification  
474 of novel genetic factors associated with brain aging. *Neurobiol. Aging* **105**, 199–204  
475 (2021).
- 476 20. Leonardsen, E. H. *et al.* Genetic architecture of brain age and its causal relations with  
477 brain and mental disorders. *Mol. Psychiatry* (2023) doi:10.1038/s41380-023-02087-y.
- 478 21. Ning, K., Zhao, L., Matloff, W., Sun, F. & Toga, A. W. Association of relative brain  
479 age with tobacco smoking, alcohol consumption, and genetic variants. *Sci. Rep.* **10**,  
480 (2020).

- 481 22. Gaser, C. *et al.* CAT { \textendash } A Computational Anatomy Toolbox for the  
482 Analysis of Structural MRI Data. *bioRxiv* (2023) doi:10.1101/2022.06.11.495736.
- 483 23. Bycroft, C. *et al.* The UK Biobank resource with deep phenotyping and genomic data.  
484 *Nature* **562**, 203–209 (2018).
- 485 24. Tipping, M. E. Sparse Bayesian Learning and the Relevance Vector Machine. *J. Mach.*  
486 *Learn. Res.* **1**, 211–244 (2001).
- 487 25. Chen, T. *et al.* xgboost: Extreme Gradient Boosting. (2019).
- 488 26. Loeffler, M. *et al.* The LIFE-Adult-Study: objectives and design of a population-based  
489 cohort study with 10,000 deeply phenotyped adults in Germany. *BMC Public Health*  
490 **15**, 691 (2015).
- 491 27. Engel, C. *et al.* Cohort Profile: The LIFE-Adult-Study. *Int. J. Epidemiol.* (2022)  
492 doi:10.1093/ije/dyac114.
- 493 28. McGraw, K. O. & Wong, S. P. Forming inferences about some intraclass correlation  
494 coefficients. *Psychol. Methods* **1**, 30–46 (1996).
- 495 29. Millard, L. A. C., Davies, N. M., Gaunt, T. R., Davey Smith, G. & Tilling, K. Software  
496 Application Profile: PHESANT: a tool for performing automated phenome scans in  
497 UK Biobank. *Int. J. Epidemiol.* **47**, 29–35 (2018).
- 498 30. Dale, A. M., Fischl, B. & Sereno, M. I. Cortical Surface-Based Analysis: I.  
499 Segmentation and Surface Reconstruction. *Neuroimage* **9**, 179–194 (1999).
- 500 31. Bulik-Sullivan, B. *et al.* LD score regression distinguishes confounding from  
501 polygenicity in genome-wide association studies. *Nat. Genet.* **47**, 291–295 (2015).
- 502 32. Yang, J., Lee, S. H., Goddard, M. E. & Visscher, P. M. GCTA: A tool for genome-wide  
503 complex trait analysis. *Am. J. Hum. Genet.* **88**, 76–82 (2011).
- 504 33. Yang, J. *et al.* Conditional and joint multiple-SNP analysis of GWAS summary  
505 statistics identifies additional variants influencing complex traits. *Nat. Genet.* **44**, 369–  
506 75, S1–3 (2012).
- 507 34. Benner, C. *et al.* FINEMAP: efficient variable selection using summary data from  
508 genome-wide association studies. *Bioinformatics* **32**, 1493–1501 (2016).
- 509 35. Wang, K., Li, M. & Hakonarson, H. ANNOVAR: functional annotation of genetic  
510 variants from high-throughput sequencing data. *Nucleic Acids Res.* **38**, e164–e164  
511 (2010).
- 512 36. Rentzsch, P., Schubach, M., Shendure, J. & Kircher, M. CADD-Splice—improving  
513 genome-wide variant effect prediction using deep learning-derived splice scores. *Genome*  
514 *Med.* **13**, 31 (2021).
- 515 37. Quang, D., Chen, Y. & Xie, X. DANN: a deep learning approach for annotating the  
516 pathogenicity of genetic variants. *Bioinformatics* **31**, 761–763 (2015).
- 517 38. Ioannidis, N. M. *et al.* REVEL: An Ensemble Method for Predicting the Pathogenicity  
518 of Rare Missense Variants. *Am. J. Hum. Genet.* **99**, 877–885 (2016).
- 519 39. Ardlie, K. G. *et al.* The Genotype-Tissue Expression (GTEx) pilot analysis: Multitissue  
520 gene regulation in humans. *Science (80-. )*. **348**, 648–660 (2015).
- 521 40. Zhu, Z. *et al.* Integration of summary data from GWAS and eQTL studies predicts  
522 complex trait gene targets. *Nat. Genet.* **48**, 481–487 (2016).
- 523 41. Wu, Y. *et al.* Integrative analysis of omics summary data reveals putative mechanisms  
524 underlying complex traits. *Nat. Commun.* **9**, 918 (2018).
- 525 42. Qi, T. *et al.* Genetic control of RNA splicing and its distinct role in complex trait  
526 variation. *Nat. Genet.* (2022) doi:10.1038/s41588-022-01154-4.
- 527 43. Weeks, E. M. *et al.* Leveraging polygenic enrichments of gene features to predict genes

- 528 underlying complex traits and diseases. *Nat. Genet.* **55**, 1267–1276 (2023).
- 529 44. Stefansson, H. *et al.* A common inversion under selection in Europeans. *Nat. Genet.* **37**,  
530 129–137 (2005).
- 531 45. Okbay, A. *et al.* Genetic variants associated with subjective well-being, depressive  
532 symptoms, and neuroticism identified through genome-wide analyses. *Nat. Genet.* **48**,  
533 624–633 (2016).
- 534 46. Sollis, E. *et al.* The NHGRI-EBI GWAS Catalog: knowledgebase and deposition  
535 resource. *Nucleic Acids Res.* **51**, D977–D985 (2023).
- 536 47. Lee, J. J. *et al.* Gene discovery and polygenic prediction from a genome-wide  
537 association study of educational attainment in 1.1 million individuals. *Nat. Genet.* **50**,  
538 1112–1121 (2018).
- 539 48. Nagel, M. *et al.* Meta-analysis of genome-wide association studies for neuroticism in  
540 449,484 individuals identifies novel genetic loci and pathways. *Nat. Genet.* **50**, 920–927  
541 (2018).
- 542 49. Karlsson Linnér, R. *et al.* Genome-wide association analyses of risk tolerance and risky  
543 behaviors in over 1 million individuals identify hundreds of loci and shared genetic  
544 influences. *Nat. Genet.* **51**, 245–257 (2019).
- 545 50. Jansen, P. R. *et al.* Genome-wide analysis of insomnia in 1,331,010 individuals  
546 identifies new risk loci and functional pathways. *Nat. Genet.* **51**, 394–403 (2019).
- 547 51. Kichaev, G. *et al.* Leveraging Polygenic Functional Enrichment to Improve GWAS  
548 Power. *Am. J. Hum. Genet.* **104**, 65–75 (2019).
- 549 52. Hollis, B. *et al.* Genomic analysis of male puberty timing highlights shared genetic basis  
550 with hair colour and lifespan. *Nat. Commun.* **11**, 1536 (2020).
- 551 53. Jun, G. *et al.* A novel Alzheimer disease locus located near the gene encoding tau  
552 protein. *Mol. Psychiatry* **21**, 108–117 (2016).
- 553 54. Rademakers, R., Cruts, M. & van Broeckhoven, C. The role of tau (MAPT) in  
554 frontotemporal dementia and related tauopathies. *Hum. Mutat.* **24**, 277–295 (2004).
- 555 55. Bittner, S., Ruck, T., Fernández-Orth, J. & Meuth, S. G. TREK-King the Blood–  
556 Brain-Barrier. *J. Neuroimmune Pharmacol.* **9**, 293–301 (2014).
- 557 56. Wang, W. *et al.* Lig4-4 selectively inhibits TREK-1 and plays potent neuroprotective  
558 roles in vitro and in rat MCAO model. *Neurosci. Lett.* **671**, 93–98 (2018).
- 559 57. van der Meer, D. *et al.* Understanding the genetic determinants of the brain with  
560 MOSTest. *Nat. Commun.* **11**, 3512 (2020).
- 561 58. Shadrin, A. A. *et al.* Vertex-wise multivariate genome-wide association study identifies  
562 780 unique genetic loci associated with cortical morphology. *Neuroimage* **244**, 118603  
563 (2021).
- 564 59. Le Guen, Y. *et al.* eQTL of KCNK2 regionally influences the brain sulcal widening:  
565 evidence from 15,597 UK Biobank participants with neuroimaging data. *Brain Struct.*  
566 *Funct.* **224**, 847–857 (2019).
- 567 60. Sharma, K., Tyagi, R., Singh, R., Sharma, S. K. & Anand, A. Serum Levels of TIMP-3,  
568 LIPC, IER3, and SLC16A8 in CFH-Negative AMD Cases. *J. Cell. Biochem.* **118**,  
569 2087–2095 (2017).
- 570 61. Zaharija, B., Samardžija, B. & Bradshaw, N. J. The TRIOBP Isoforms and Their  
571 Distinct Roles in Actin Stabilization, Deafness, Mental Illness, and Cancer. *Molecules*  
572 **25**, (2020).
- 573 62. Vujkovic, M. *et al.* Discovery of 318 new risk loci for type 2 diabetes and related  
574 vascular outcomes among 1.4 million participants in a multi-ancestry meta-analysis.  
575 *Nat. Genet.* **52**, 680–691 (2020).

- 576 63. Sakaue, S. *et al.* A cross-population atlas of genetic associations for 220 human  
577 phenotypes. *Nat. Genet.* **53**, 1415–1424 (2021).
- 578 64. Malik, T. H. *et al.* Transcriptional repression and developmental functions of the  
579 atypical vertebrate GATA protein TRPS1. *EMBO J.* **20**, 1715–1725 (2001).
- 580 65. Qi, T. *et al.* Identifying gene targets for brain-related traits using transcriptomic and  
581 methylomic data from blood. *Nat. Commun.* **9**, 2282 (2018).
- 582 66. Cheung, C. T., Kaul, S. C. & Wadhwa, R. Molecular bridging of aging and cancer.  
583 *Ann. N. Y. Acad. Sci.* **1197**, 129–133 (2010).
- 584 67. Fjorback, A. W., Müller, H. K. & Wiborg, O. Membrane glycoprotein M6B interacts  
585 with the human serotonin transporter. *J. Mol. Neurosci.* **37**, 191–200 (2009).
- 586 68. Zhang, G. *et al.* DHRSX, a novel non-classical secretory protein associated with  
587 starvation induced autophagy. *Int. J. Med. Sci.* **11**, 962–970 (2014).
- 588 69. Bakshi, A. *et al.* Fast set-based association analysis using summary data from GWAS  
589 identifies novel gene loci for human complex traits. *Sci. Rep.* **6**, 1–9 (2016).
- 590 70. Jansen, I. E. *et al.* Genome-wide meta-analysis identifies new loci and functional  
591 pathways influencing Alzheimer’s disease risk. *Nat. Genet.* **51**, 404–413 (2019).
- 592 71. Ashburner, M. *et al.* Gene Ontology: tool for the unification of biology. *Nat. Genet.* **25**,  
593 25–29 (2000).
- 594 72. Grote, S. GOfuncR: Gene ontology enrichment using FUNC. (2021).
- 595 73. Takai, Y., Sasaki, T. & Matozaki, T. Small GTP-binding proteins. *Physiol. Rev.* **81**,  
596 153–208 (2001).
- 597 74. Reiner, D. J. & Lundquist, E. A. Small GTPases. *WormBook: the online review of C.*  
598 *elegans biology* vol. 2018 1–65 (2018).
- 599 75. Wennerberg, K., Rossman, K. L. & Der, C. J. The Ras superfamily at a glance. *J. Cell*  
600 *Sci.* **118**, 843–846 (2005).
- 601 76. Ejaz, A., Mattesich, M. & Zwerschke, W. Silencing of the small GTPase DIRAS3  
602 induces cellular senescence in human white adipose stromal/progenitor cells. *Aging*  
603 (*Albany, NY*). **9**, 860–879 (2017).
- 604 77. Wang, L., Yang, L., Debidda, M., Witte, D. & Zheng, Y. Cdc42 GTPase-activating  
605 protein deficiency promotes genomic instability and premature aging-like phenotypes.  
606 *Proc. Natl. Acad. Sci. U. S. A.* **104**, 1248–1253 (2007).
- 607 78. Debidda, M., Williams, D. A. & Zheng, Y. Rac1 GTPase regulates cell genomic  
608 stability and senescence. *J. Biol. Chem.* **281**, 38519–38528 (2006).
- 609 79. Bulik-Sullivan, B. *et al.* An atlas of genetic correlations across human diseases and  
610 traits. *Nat. Genet.* **47**, 1236–1241 (2015).
- 611 80. Abdellaoui, A. & Verweij, K. J. H. Dissecting polygenic signals from genome-wide  
612 association studies on human behaviour. *Nat. Hum. Behav.* **5**, 686–694 (2021).
- 613 81. Abdellaoui, A. *et al.* Genetic correlates of social stratification in Great Britain. *Nat.*  
614 *Hum. Behav.* **3**, 1332–1342 (2019).
- 615 82. Wray, N. R. *et al.* Genome-wide association analyses identify 44 risk variants and  
616 refine the genetic architecture of major depression. *Nat. Genet.* **50**, 668–681 (2018).
- 617 83. Zhu, Z. *et al.* Causal associations between risk factors and common diseases inferred  
618 from GWAS summary data. *Nat. Commun.* **9**, 224 (2018).
- 619 84. Evangelou, E. *et al.* Genetic analysis of over 1 million people identifies 535 new loci  
620 associated with blood pressure traits. *Nat. Genet.* **50**, 1412–1425 (2018).
- 621 85. Wu, W. *et al.* An electroencephalographic signature predicts antidepressant response in  
622 major depression. *Nat. Biotechnol.* 1–9 (2020) doi:10.1038/s41587-019-0397-3.

- 623 86. Wood, A. R. *et al.* Defining the role of common variation in the genomic and biological  
624 architecture of adult human height. *Nat. Genet.* **46**, 1173–1186 (2014).
- 625 87. Baselmans, B. M. L. *et al.* Multivariate genome-wide analyses of the well-being  
626 spectrum. *Nat. Genet.* **51**, 445–451 (2019).
- 627 88. Montag, C., Ebstein, R. P., Jawinski, P. & Markett, S. Molecular genetics in  
628 psychology and personality neuroscience: On candidate genes, genome wide scans, and  
629 new research strategies. *Neuroscience and Biobehavioral Reviews* vol. 118 163–174  
630 (2020).
- 631 89. Zhang, Y., Qi, G., Park, J. H. & Chatterjee, N. Estimation of complex effect-size  
632 distributions using summary-level statistics from genome-wide association studies across  
633 32 complex traits. *Nat. Genet.* **50**, 1318–1326 (2018).
- 634 90. Gaser, C., Franke, K., Klöppel, S., Koutsouleris, N. & Sauer, H. BrainAGE in Mild  
635 Cognitive Impaired Patients: Predicting the Conversion to Alzheimer’s Disease. *PLoS*  
636 *One* **8**, e67346 (2013).
- 637 91. Savage, J. E. *et al.* Genome-wide association meta-analysis in 269,867 individuals  
638 identifies new genetic and functional links to intelligence. *Nat. Genet.* **50**, 912–919  
639 (2018).
- 640 92. Vidal-Piñeiro, D. *et al.* Individual variations in “Brain age” relate to early life factors  
641 more than to longitudinal brain change. *bioRxiv* 2021.02.08.428915 (2021)  
642 doi:10.1101/2021.02.08.428915.
- 643 93. Frei, O. *et al.* Bivariate causal mixture model quantifies polygenic overlap between  
644 complex traits beyond genetic correlation. *Nat. Commun.* **10**, 2417 (2019).
- 645 94. Larstone, R. M., Jang, K. L., Livesley, W. J., Vernon, P. A. & Wolf, H. The  
646 relationship between Eysenck’s P-E-N model of personality, the five-factor model of  
647 personality, and traits delineating personality dysfunction. *Pers. Individ. Dif.* **33**, 25–37  
648 (2002).
- 649 95. Franke, K., Ziegler, G., Klöppel, S. & Gaser, C. Estimating the age of healthy subjects  
650 from T1-weighted MRI scans using kernel methods: Exploring the influence of various  
651 parameters. *Neuroimage* **50**, 883–892 (2010).
- 652 96. Franke, K., Luders, E., May, A., Wilke, M. & Gaser, C. Brain maturation: Predicting  
653 individual BrainAGE in children and adolescents using structural MRI. *Neuroimage*  
654 **63**, 1305–1312 (2012).
- 655 97. Franke, K. & Gaser, C. Longitudinal changes in individual BrainAGE in healthy aging,  
656 mild cognitive impairment, and Alzheimer’s Disease. *GeroPsych J. Gerontopsychology*  
657 *Geriatr. Psychiatry* **25**, 235–245 (2012).
- 658 98. Qiu, K. Relevance Vector Machine (RVM). (2019).
- 659 99. Chen, T. & Guestrin, C. XGBoost: A Scalable Tree Boosting System. in *Proceedings of*  
660 *the 22nd ACM SIGKDD International Conference on Knowledge Discovery and Data*  
661 *Mining* 785–794 (Association for Computing Machinery, 2016).  
662 doi:10.1145/2939672.2939785.
- 663 100. Larivière, S. *et al.* The ENIGMA Toolbox: multiscale neural contextualization of  
664 multisite neuroimaging datasets. *Nat. Methods* **18**, 698–700 (2021).
- 665 101. Welsh, S., Peakman, T., Sheard, S. & Almond, R. Comparison of DNA quantification  
666 methodology used in the DNA extraction protocol for the UK Biobank cohort. *BMC*  
667 *Genomics* **18**, 26 (2017).
- 668 102. Manichaikul, A. *et al.* Robust relationship inference in genome-wide association studies.  
669 *Bioinformatics* **26**, 2867–2873 (2010).
- 670 103. Galinsky, K. J. *et al.* Fast principal-component analysis reveals convergent evolution of

- 671 ADH1B in Europe and East Asia. *Am. J. Hum. Genet.* **98**, 456–472 (2016).
- 672 104. Jawinski, P. *et al.* Human brain arousal in the resting state: a genome-wide association  
673 study. *Mol. Psychiatry* **24**, 1599–1609 (2019).
- 674 105. Chang, C. C. *et al.* Second-generation PLINK: rising to the challenge of larger and  
675 richer datasets. *Gigascience* **4**, s13742–015 (2015).
- 676 106. Yang, J. *et al.* Common SNPs explain a large proportion of the heritability for human  
677 height. *Nat. Genet.* **42**, 565–569 (2010).
- 678 107. Finucane, H. K. *et al.* Partitioning heritability by functional annotation using genome-  
679 wide association summary statistics. *Nat. Genet.* **47**, 1228–1235 (2015).
- 680 108. Gazal, S. *et al.* Functional architecture of low-frequency variants highlights strength of  
681 negative selection across coding and non-coding annotations. *Nat. Genet.* **50**, 1600–  
682 1607 (2018).
- 683 109. Benjamini, Y. & Hochberg, Y. Controlling the False Discovery Rate: A Practical and  
684 Powerful Approach to Multiple Testing. *J. R. Stat. Soc.* **57**, 289–300 (1995).
- 685 110. Willer, C. J., Li, Y. & Abecasis, G. R. METAL: fast and efficient meta-analysis of  
686 genomewide association scans. *Bioinformatics* **26**, 2190–2191 (2010).
- 687 111. Visscher, P. M. *et al.* 10 Years of GWAS Discovery: Biology, Function, and  
688 Translation. *Am. J. Hum. Genet.* **101**, 5–22 (2017).
- 689 112. Adhikari, K. R Functions to calculate power of GWAS studies.  
690 <https://github.com/kaustubhad/gwas-power> (2018).
- 691 113. Palmer, C. & Pe'er, I. Statistical correction of the Winner's Curse explains replication  
692 variability in quantitative trait genome-wide association studies. *PLOS Genet.* **13**,  
693 e1006916 (2017).
- 694 114. Watanabe, K., Taskesen, E., van Bochoven, A. & Posthuma, D. Functional mapping  
695 and annotation of genetic associations with FUMA. *Nat. Commun.* **8**, 1826 (2017).
- 696 115. Benner, C. *et al.* Prospects of Fine-Mapping Trait-Associated Genomic Regions by  
697 Using Summary Statistics from Genome-wide Association Studies. *Am. J. Hum.*  
698 *Genet.* **101**, 539–551 (2017).
- 699 116. Benner, C., Havulinna, A. S., Salomaa, V., Ripatti, S. & Pirinen, M. Refining fine-  
700 mapping: effect sizes and regional heritability. *bioRxiv* (2018) doi:10.1101/318618.
- 701 117. O'Leary, N. A. *et al.* Reference sequence (RefSeq) database at NCBI: current status,  
702 taxonomic expansion, and functional annotation. *Nucleic Acids Res.* **44**, D733-45  
703 (2016).
- 704 118. Nassar, L. R. *et al.* The UCSC Genome Browser database: 2023 update. *Nucleic Acids*  
705 *Res.* **51**, D1188–D1195 (2023).
- 706 119. Liu, X., Wu, C., Li, C. & Boerwinkle, E. dbNSFP v3.0: A One-Stop Database of  
707 Functional Predictions and Annotations for Human Nonsynonymous and Splice-Site  
708 SNVs. *Hum. Mutat.* **37**, 235–241 (2016).
- 709 120. Aguet, F. *et al.* Genetic effects on gene expression across human tissues. *Nature* **550**,  
710 204–213 (2017).
- 711 121. Durinck, S., Spellman, P. T., Birney, E. & Huber, W. Mapping identifiers for the  
712 integration of genomic datasets with the R/Bioconductor package biomaRt. *Nat.*  
713 *Protoc.* **4**, 1184–1191 (2009).
- 714 122. Team, B. C. Homo.sapiens: Annotation package for the Homo.sapiens object. (2015).
- 715 123. Carlson, M. GO.db: A set of annotation maps describing the entire Gene Ontology.  
716 (2021).
- 717 124. Alexa, A., Rahnenführer, J. & Lengauer, T. Improved scoring of functional groups from

- 718 gene expression data by decorrelating GO graph structure. *Bioinformatics* **22**, 1600–  
719 1607 (2006).
- 720 125. Choi, S. W. & O’Reilly, P. F. PRSice-2: Polygenic Risk Score software for biobank-  
721 scale data. *Gigascience* **8**, giz082 (2019).
- 722 126. Consortium, S. W. G. of the P. G. *et al.* Biological insights from 108 schizophrenia-  
723 associated genetic loci. *Nature* **511**, 421 (2014).
- 724 127. Zhang, Y., Qi, G., Park, J. H. & Chatterjee, N. Estimation of complex effect-size  
725 distributions using summary-level statistics from genome-wide association studies across  
726 32 complex traits. *Nat. Genet.* **50**, 1318–1326 (2018).
- 727 128. Allen, H. L. *et al.* Hundreds of variants clustered in genomic loci and biological  
728 pathways affect human height. *Nature* **467**, 832–838 (2010).
- 729



## 730 **Methods**

### 731 **Sample characteristics**

732 Participants were drawn from the UK Biobank cohort study ([www.ukbiobank.ac.uk](http://www.ukbiobank.ac.uk)) under  
733 application number 423032. A detailed description of the UK Biobank study design, participants  
734 and quality control (QC) methods has been published previously.<sup>23</sup> The UKB received ethical  
735 approval from the National Research Ethics Service Committee North West-Haydock (reference  
736 11/NW/0382). All participants provided written informed consent. In the current study, the  
737 majority of participants were drawn from the January 2020 UKB brain imaging release (v1.7).  
738 These data contained 40,681 participants with structural T1-weighted MRI data (UKB data-  
739 field 20252). We did not include T1-weighted MRI scans in folders labelled as ‘unusable’ (leaving  
740 39,679 participants). In total, MRI scans of 39,677 participants completed the voxel-based  
741 morphometry preprocessing (see section ‘MRI acquisition and preprocessing’). Analyses were  
742 restricted to participants whose self-reported sex matched the genetic sex (data-field 31 and  
743 2200), who were without indications of sex aneuploidy (data-field 22019), and who were no  
744 outliers in heterozygosity and missingness (data-field 22027). We only included unrelated  
745 participants as suggested by pairwise kinship coefficients below 0.0442 (pre-calculated  
746 coefficients retrieved using the command line tool ‘ukbgene’ with the ‘rel’ parameter). In our  
747 discovery GWAS, we only included participants of white-British ancestry (data-field 22006),  
748 which resulted in a final discovery sample of 32,634 participants (17,084 female, age range: 45.2-  
749 81.9 years, mean age: 64.3 years).

750 For replication analyses, we selected all remaining non-white-British ancestry individuals  
751 of the January 2020 release. Applying the same inclusion criteria, we then added participants  
752 whose imaging data were released until September 2022 (release v1.9), yielding a total of 7,785  
753 additional individuals. None of these individuals were related to individuals in the discovery  
754 sample. We only included individuals with a valid ancestry assignment from the Pan-ancestry  
755 UKB project (UKB return 2442; <https://pan.ukbb.broadinstitute.org/>). This resulted in 217  
756 African, 60 Admixed American, 409 Central/South Asian, 192 East Asian, 4,486 European, and  
757 62 Middle Eastern ancestry participants. In total, we included 5,427 UKB participants for  
758 replication analyses (2,847 female, age range: 44.6-82.8 years, mean age: 65.9 years). From the  
759 LIFE-Adult cohort study,<sup>26,27</sup> we included another 1,833 European ancestry participants  
760 (888 female, age range: 45.2-80.3 years, mean age: 65.3 years).<sup>26,27</sup> Altogether, the final  
761 replication sample included 7,259 participants (3,735 female, age range: 44.6-82.8 years, mean  
762 age: 65.7 years) from 7 subsamples (see section ‘Genome-wide association analysis and replication  
763 meta-analysis meta-analysis’ for analysis details).

## 764 **MRI data acquisition**

765 The UKB imaging acquisition protocol and processing pipeline have been detailed previously  
766 (<http://biobank.ctsu.ox.ac.uk/crystal/refer.cgi?id=1977>). In brief, brain MRI data were  
767 acquired in one of four UKB imaging centers (Cheadle, Newcastle, Reading, and Bristol) on  
768 Siemens Skyra 3T MRI scanners (Siemens Healthcare, Erlangen, Germany), running software  
769 VD13A SP4 with a standard Siemens 32-channel RF receive head coil. UKB's neuroimaging  
770 strategy includes the acquisition of several imaging modalities. In this study, we used T1-  
771 weighted structural MRI scans acquired using a 3D MPRAGE sequence in the sagittal plane,  
772 with 1x1x1 mm voxel-size, 208x256x256 acquisition matrix, 2,000 ms repetition time (TR),  
773 2.01 ms echo time (TE), 880 ms inversion time (TI), 6.1 ms echo spacing, 8° flip angle,  
774 240 Hz/pixel bandwidth, in-plane acceleration factor of  $R = 2$ , and 4:54 min duration  
775 (<https://www.fmrib.ox.ac.uk/ukbiobank/protocol/>). T1-weighted scans were defaced for subject  
776 anonymity and made available in NIFTI format (data-field 20252).

777 In LIFE-Adult, brain imaging was performed using a 3T Siemens Verio MRI scanner  
778 (Siemens Healthcare, Erlangen, Germany) equipped with a standard 32 channel head coil. High  
779 resolution T1-weighted structural images were obtained using a 3D MPRAGE sequence with  
780 1x1x1 mm voxel-size, 256x240x176 acquisition matrix, TR = 2,300 ms, TE = 2.98 ms, TI = 900  
781 ms, and 9° flip angle.

## 782 **MRI preprocessing**

783 T1-weighted MRI scans in NIFTI-format were preprocessed using the voxel-based morphometry  
784 pipeline of CAT12 (r1364, <http://dbm.neuro.uni-jena.de>) for SPM12 (r7487) in MATLAB  
785 R2021a (The MathWorks Inc, Natick, MA, USA). CAT12 preprocessing involved affine and  
786 DARTEL registration of brain images to a reference brain, segmentation into grey matter, white  
787 matter, and cerebro-spinal fluid, bias correction for intensity inhomogeneity, and modulation of  
788 segmentations to account for the amount of volume changes due to spatial registration. Processed  
789 images were smoothed by applying an 8x8x8mm full-width-at-half-maximum (FWHM) gaussian  
790 kernel with subsequent resampling to 8mm<sup>3</sup> voxel size. We only considered MRI scans with a  
791 CAT12 overall image quality rating < 3.0 for further downstream analyses.

## 792 **Feature set for machine learning**

793 The feature set for machine learning was derived from CAT12-preprocessed grey and white  
794 matter segmentations, with the smoothed and resampled brain images comprising 16128 voxels  
795 each. We excluded voxels that did not show any variation across individuals, resulting in 5416  
796 voxels for grey matter images and 5123 voxels for white matter images. Typically, voxel-based  
797 images are characterized by substantial spatial correlations. We conducted principal component  
798 analysis (PCA) in MATLAB to remove redundant information and reduce dimensionality. We

799 selected the first 500 principal components as features, which explained about 90% of the total  
800 variance in brain images and enabled model training in a reasonable period of time with advanced  
801 computational resources.

## 802 **Machine learning algorithms**

803 Age estimation models were built using the sparse Bayesian relevance vector machine (RVM) in  
804 MATLAB (The MathWorks Inc, Natick, MA, USA),<sup>24</sup> and the extreme gradient boosting  
805 package ‘xgboost’ v.0.82.1 in R.<sup>25,94</sup> The RVM was developed as a probabilistic Bayesian  
806 equivalent to the popular support vector regression (SVR), and has widely been used in brain  
807 age research.<sup>95–97</sup> We used the RVM implemented in MATLAB toolbox SparseBayes v.2 with  
808 the wrapper and kernel function by Qiu.<sup>98</sup> Furthermore, we made use of the XGBoost algorithms,  
809 which have become popular methods after winning several machine learning challenges hosted  
810 by the data science competition platform Kaggle.<sup>25,99</sup> XGBoost has previously been employed in  
811 brain age research.<sup>15</sup> We used XGBoost with both the decision tree (‘gbtree’) and linear gradient  
812 booster (‘gblinear’). The learning rate was set to  $\eta = 0.02$  with 5000 training iterations and an  
813 early stopping after 50 iterations in the case of no further model improvement. The maximum  
814 tree depth was set to 3. Default settings were used for all other training parameters.

## 815 **Model training and age prediction**

816 Age estimation models were trained with the brain image PCA scores serving as features and  
817 chronological age serving as outcome variable. Model training and application was carried out  
818 in a 10-fold cross-validation manner with 100 repeats. Therefore, we randomly split the discovery  
819 sample into ten equal-sized subsets, of which nine subsets served for model training, and the  
820 remaining subset, the test sample, served for applying the model. Brain images of the training  
821 sample underwent PCA, and transformation parameters were subsequently applied to calculate  
822 PCA scores in the test sample. After the first model was trained and tested, the next subset  
823 served as test sample, while the other nine subsets were selected as training sample. This strategy  
824 was carried on until each subset served exactly once as test sample. The tenfold cross-validation  
825 procedure was repeated 100 times, so that 100 predictions were made for each subject. This  
826 procedure was performed for each tissue (grey and white matter) and model type (relevance  
827 vector machine, xgboost tree, and xgboost linear), resulting in a total number of 600 brain-  
828 predicted age estimates per subject. In a nested 10-fold cross-validation approach, we stacked  
829 the estimates from the three different model types in an ensemble estimate, resulting in 100  
830 brain-predicted age estimates for grey matter, white matter, and combined grey and white  
831 matter, respectively. Finally, these estimates were averaged, leaving one brain-predicted age  
832 estimate for grey matter, white matter, and combined grey and white matter for each subject.

833 In the replication samples, we employed all discovery models from the 10-fold cross-  
834 validation procedure and compared the resulting age predictions against those derived from  
835 additional models where the complete discovery sample was used for model training. Results  
836 were highly concordant for all three tissue classes ( $r > .997$ ). Due to the improved practicability,  
837 we performed subsequent replication analyses based on models trained on the complete discovery  
838 sample, which revealed virtually identical age predictions.

### 839 **Cross-trait association analysis**

840 Cross-trait association analyses were carried out using PHESANT,<sup>29</sup> an automated  
841 preprocessing and analysis pipeline for phenome-wide association analyses in UK Biobank  
842 datasets. Cross-trait associations were conducted for each BAG trait and 7,088 non-imaging  
843 derived UK Biobank variables. Sex, age, age<sup>2</sup>, scanner site, and total intracranial volume served  
844 as covariates. Based on variable type (continuous, integer, categorical single choice, or  
845 categorical multiple choice) and number of distinct values observed, different types of regression  
846 analyses (linear, logistic, ordinal logistic, or multinomial logistic) were performed. Variables  
847 suitable for linear regression underwent inverse-rank normal transformation. To obtain  
848 standardized effect size estimates, we converted the resulting beta coefficients from the different  
849 types of regression models to a corresponding correlation coefficient  $r$  based on  $p$ -value, number  
850 of observations, and number of covariates. Phenome-wide association analysis plots were created  
851 by assigning each variable to a custom UK Biobank category based on the respective variable's  
852 UK Biobank data dictionary path.

### 853 **FreeSurfer associations**

854 In addition to PheWAS analyses of non-imaging-derived phenotypes, we associated BAG with  
855 brain measures derived from the FreeSurfer `aparc` and `aseg` output files.<sup>30</sup> FreeSurfer is an open-  
856 source software package to process, analyze and visualize human brain MR images. We retrieved  
857 FreeSurfer output files from the UKB resource (data-field 20263) and extracted surface area,  
858 cortical thickness, and cortical volume estimates of 34 bilateral cortical segmentations, as well  
859 as volume estimates of 8 bilateral subcortical segmentations, resulting in 220 brain measures in  
860 total. We calculated partial product-moment correlations between BAG and the 220 brain  
861 measures using sex, age, age<sup>2</sup>, scanner site, and total intracranial volume as covariates.  
862 Visualizations were performed using the ENIGMA toolbox.<sup>100</sup>

### 863 **UKB genotyping and imputation**

864 We retrieved called and imputed genotypes (version 3) in BED and BGEN format, respectively,  
865 from the UK Biobank resource. Genotype collection, processing, and quality control have  
866 previously been described in detail.<sup>23,101</sup> In brief, DNA was extracted from EDTA-treated whole-

867 blood samples, aliquoted across three tubes (primary storage, backup storage, and genotyping  
868 tube), and shipped on 96-well plates of 50  $\mu$ L aliquot per sample for genotyping to the Affymetrix  
869 Research Services Lab, Santa Clara, CA, USA. Genotyping was carried out using two arrays  
870 with a 95% marker overlap: the Applied Biosystems UK BiLEVE Axiom Array (807,411  
871 markers; used in 49,950 participants) and the Applied Biosystems UK Biobank Axiom Array  
872 (825,927 markers; used in 438,427 participants). Both genotyping arrays were designed for  
873 genome-wide coverage of genetic content including biallelic single nucleotide polymorphisms  
874 (SNPs) and short insertions and deletions (indels). Marker-based quality control included testing  
875 for batch, plate, array, and sex effects, departures from Hardy-Weinberg-Equilibrium, as well as  
876 discordance across two control DNA replicates from the 1000 Genomes project, with two wells  
877 on each plate assigned to these control subjects. Sample-based quality control included missing  
878 rates ( $> 0.05$ ), unusually high fractions of heterozygous variant calls, and sex chromosome  
879 aneuploidy. Relatedness between individuals was inferred from kinship coefficients estimated  
880 using KING.<sup>102</sup> Population stratification was measured by applying fastPCA<sup>103</sup> Principal  
881 Component Analysis on a set of 147,604 pruned high-quality markers. White-British ancestry  
882 (data-field 22006) was derived from a combination of self-report and genetic principal  
883 components. Genotype calls were phased using SHAPEIT3 and imputation was done using  
884 IMPUTE4 (<https://jmarchini.org/software/>) with the Haplotype Reference Consortium,  
885 UK10K, and 1000 Genomes phase 3 datasets serving as reference panels. Imputation resulted in  
886  $\sim 97$ M markers available for downstream analyses.

### 887 **LIFE-Adult genotyping and imputation**

888 Genotype collection, processing, and quality control in LIFE-Adult have previously been  
889 described in detail.<sup>104</sup> DNA was extracted from peripheral blood leukocytes. Genotyping was  
890 carried out using the Applied Biosystems Axiom Genome-Wide CEU 1 Array Plate with 587,352  
891 markers. Marker-based quality control included call rate  $< 0.97$ , Hard-Weinberg equilibrium  
892  $p < 1.0e-06$ , and plate association  $p < 1.0e-07$ . Sample quality control included dish-QC  $< 0.82$ ,  
893 missing rates  $> 0.03$ , reported vs. genetic sex mismatch, and cryptic relatedness. Genotypes were  
894 pre-phased using SHAPEIT. Imputation was carried out using IMPUTE2 with the 1000 genome  
895 phase 3 dataset serving as reference. This resulted in 85,063,807 markers derived from 7,776  
896 individuals. Post-imputation quality control included MAF  $\geq 0.01$  and INFO  $\geq 0.8$ . As LIFE-  
897 Adult replication results were aggregated meta-analytically with the UKB replication results, we  
898 only included variants identified as biallelic SNPs or indels with INFO  $\geq 0.8$  in the UKB dataset

899 (see ‘UKB genotyping and imputation’). This resulted in 9,472,504 markers passing quality-  
900 control in LIFE-Adult.

### 901 **Control for population structure**

902 In the discovery sample, we calculated 20 genetic principal components by applying the  
903 randomized PCA algorithm (--pca 20 approx) implemented in PLINK v2.00a2LM 64-bit Intel  
904 (31 Jul 2019)<sup>105</sup> on the same variants used by the UKB group (resource 1955; 146,988 markers  
905 passing our own quality-checks). For the UKB replication samples, we used genetic principal  
906 components provided by the pan-ancestry UKB project (UKB return 2442). The number of  
907 principal components serving as covariates was adjusted to the respective replication sample  
908 size. We used 10 principal components as covariates in the larger European-ancestry UKB  
909 replication sample and 3 principal components in each of the other UKB replication samples. In  
910 LIFE-Adult, 4 genetic principal components were used to account for subpopulation structure.

### 911 **Heritability and partitioned heritability**

912 Estimates of SNP-based heritability ( $h^2_{\text{SNP}}$ ) were derived by applying the GCTA genomic-  
913 restricted maximum likelihood (GREML) algorithm to genetic relatedness matrices  
914 (GRMs).<sup>32,106</sup> GRMs were calculated based on biallelic autosomal variants with  $\text{MAF} \geq 0.01$   
915 and  $\text{INFO} \geq 0.80$ . GREML analyses were run in the discovery sample, with sex, age, age<sup>2</sup>,  
916 genotyping array, scanner site, total intracranial volume, and the first 20 genetic principal  
917 component serving as covariates. We conducted LD score regression<sup>31,79</sup> on the GWAS summary  
918 statistics to corroborate GREML heritability estimates. We used precalculated LD scores and  
919 regression weights from 10000 Genomes phase 3 European ancestry samples  
920 (eur\_w\_ld\_chr.tar.bz2). We retained variants with  $\text{MAF} > 0.01$  included in the HapMap3  
921 panel after removal of the MHC region (w\_hm3.noMHC.snplist.zip). In order to partition  
922 heritability by functional annotation, we conducted stratified LD score regression<sup>107</sup> using the  
923 baseline-LD model v.2.2 with the 1000 genomes phase 3 regression weights and allele frequencies  
924 excluding the MHC region. We considered functional annotations reported among the 33 ‘main  
925 annotations’ by Gazal and colleagues.<sup>108</sup> Annotations with  $\text{FDR} < 0.05$  were regarded as  
926 significant after multiple testing correction.<sup>109</sup>

### 927 **Genome-wide association analysis and replication meta-analysis**

928 GWAS analysis were run in PLINK v2.00a2LM (31 Jul 2019) based on allelic dosage data. We  
929 included autosomal (chr1-22), gonosomal (chrX and chrY), pseudoautosomal (chrXY), and  
930 mitochondrial variations (chrMT). Analyses were run with male and female dosage data on a 0-  
931 2 scale on diploid chromosomes (chr1-22, chrXY), 0-1 scale on regular haploid chromosomes  
932 (chrY and chrMT), and 0-2 scale on chrX. We selected biallelic SNPs and INDELs with

933 MAF > 0.01 and INFO > 0.80. Biallelic variations were defined as variations without duplicate  
934 chromosomal coordinates and duplicate identifiers in the imputed variant files. We modelled  
935 additive genetic effects and used sex, age, age<sup>2</sup>, total intra-cranial volume, scanner site, type of  
936 genotyping array, and the first 20 genetic principal components as covariates (3-10 genetic  
937 principal components were used in the replication GWASs; see section ‘control of population  
938 structure’). In total, there were 9,669,404 markers available for the discovery GWAS in  
939  $n = 32,634$  white-British ancestry individuals. The number of markers passing quality-control  
940 in the replication GWASs ranged between 8,364,077 (East-Asian ancestry) and 15,302,441  
941 (African ancestry). Results of the ancestry-stratified replication GWASs were aggregated by  
942 performing a fixed-effects inverse-variance-weighted meta-analysis in METAL.<sup>110</sup> Variants with  
943 an aggregated  $n$  lower than 67% of the 90th quantile of all observed  $n$  (adapted from LDSC)<sup>31</sup>  
944 and heterogeneity  $p < 1.0e-06$  were discarded. This yielded replication meta-analysis results from  
945 9,496,239 (grey matter), 9,496,243 (white matter), and 9,496,192 (grey and white matter)  
946 variants in up to  $n = 7,259$  individuals.

#### 947 **Identification of independent discoveries**

948 In order to identify independently associated variations, we performed stepwise conditional  
949 analyses employing the COJO module in GCTA.<sup>32,33</sup> We used a 10,000 kb window-size  
950 (`--cojo-wind 10000`), a collinearity cutoff of 0.9 (`--cojo-collinear 0.9`) and included variants  
951 reaching at least suggestive evidence in the discovery GWAS (`--cojo-p 1e-6`). We only considered  
952 multiple signals within one locus to be independent if the  $p$ -value of the subsidiary association  
953 signal did not increase by more than two orders of magnitudes. Variants were regarded as  
954 independent genome-wide significant discoveries if they reached  $p < 5.0e-08$  in conditional  
955 analysis. All other variants with conditional  $p < 1.0e-06$  were regarded as suggestive signals,  
956 which were not considered for fine mapping but tested for result consistency in replication  
957 analyses. We denote variants discovered through conditional analyses as ‘index variants’ (i.e.,  
958 the top variant of an association signal). To identify independent discoveries across the three  
959 BAG GWAS, we selected all index variants identified through trait-wise conditional analyses  
960 and clumped these variants according to chromosomal position and linkage disequilibrium using  
961 PLINK v1.90b6.8 (`--clump-r2 0.1 --clump-kb 10000`).

#### 962 **Definition of variant replication and power calculations**

963 For replication analyses, we selected index variations from genome-wide significant loci  
964 ( $p < 5.0e-08$ ), and index variations from another 45 suggestive loci (conditional  $p$ -values ranging  
965 from  $1.0e-06$  to  $5.0e-08$ ). Consistency between discovery and replication results were tested via  
966 sign tests, i.e., binomial tests based on the number of observations where replication effect  
967 directions agree with the corresponding discovery effect directions. Variants with replication

968  $p < 0.05$  (one-tailed nominal significance) were regarded as replicated variants. To estimate the  
969 expected number of successful replications, we carried out power calculations based on  
970 standardized beta coefficients (discovery), MAF (discovery), and N (replication).<sup>111,112</sup> Beta  
971 coefficients were corrected for winner's curse.<sup>113</sup> The expected number of successful replications  
972 was calculated as sum of all power values obtained for each individual variant.

### 973 **Novelty of the discovered loci**

974 Novelty of the discovered loci was examined by comparing our results against four previous  
975 genetic studies on BAG reporting discoveries at genome-wide significance levels.<sup>17,18,20,21</sup> We used  
976 the clumping algorithm in PLINK v1.90b6.8 and regarded our own discoveries as novel if they  
977 did not clump together with previously reported variants, using a linkage disequilibrium  
978 threshold of  $R^2 = 0.1$  and a clumping window of 10 Mbp (--clump-r2 0.1 --clump-kb 10000).

### 979 **ANNOVAR enrichment test**

980 We used the ANNOVAR (2017-07-17)<sup>35</sup> enrichment test implemented in FUMA v.1.3.7, a web-  
981 based platform to functionally map and annotate GWAS results (<https://fuma.ctglab.nl/>),<sup>114</sup>  
982 to test if genome-wide significant regions include relatively high or low proportions of variants  
983 with certain functional annotations. All candidate variants in linkage disequilibrium with an  
984 independent significant variant were considered for the ANNOVAR enrichment test.  
985 Independent significant variants were defined as autosomal variants reaching  $p < 5.E-08$  and  
986 clumped with an  $r^2$  threshold of 0.60. Candidate variants were defined as all variants reaching  
987  $p < 0.05$  and showing  $r^2 \geq 0.60$  with an independent significant variant. UK Biobank release2  
988 served as reference panel. If variants were annotated with multiple functional categories, each  
989 category was counted as distinct annotation. Enrichment was computed as the proportion of  
990 variants with a certain annotation divided by the proportion of variants with that annotation  
991 relative to all available SNPs in the reference panel. A two-tailed Fisher's exact test was  
992 conducted to test significance.

### 993 **Credible sets of variants**

994 For each locus identified for the three BAG traits, we used FINEMAP<sup>34</sup> v.1.4.1 to construct  
995 credible sets of variants that cumulatively capture 95% of the regional posterior probability to  
996 include the causal variant. FINEMAP uses a Bayesian framework and a computationally efficient  
997 shotgun stochastic search algorithm to model the LD structure and the strength of the variants'  
998 associations ( $Z$  scores) to infer likely causal variants. For each locus, we used a 5 Mb window  
999 around the index variant to identify the furthest variants in linkage disequilibrium ( $R^2 \geq 0.1$ )  
1000 with the index variation. Base pair positions of the identified variants were used as lower and  
1001 upper bound of the respective genomic region. LD matrices covering all variants within that



1002 genomic region were calculated by applying LDstore<sup>115</sup> v2.0 to the same allelic dosage data as  
1003 employed for the genome-wide association analysis. We then applied FINEMAP allowing for up  
1004 to  $k=10$  causal variants within each region ('--sss --n-causal-snps 10 --prob-cred-set 0.95').  
1005 Expected numbers of causal variants were derived by multiplying each evaluated number of  $k$   
1006 causal variants by the FINEMAP model-based probability. We report 95% credible sets for the  
1007 most probable  $k$  model and report all variants that have been included in one of the credible  
1008 sets for the  $k$  causal signals. We also report the FINEMAP model-averaged regional heritability,  
1009 i.e., the estimated phenotypic variance explained by causal variants within each genomic  
1010 region.<sup>116</sup>

### 1011 **Functional annotation of variants**

1012 Annotation of variants was carried out using ANNOVAR,<sup>35</sup> which allows to assign functional  
1013 categories to variants through their physical position relative to defined genes. We used RefSeq  
1014 gene annotations in human genome build 19 (hg19)<sup>117</sup> retrieved from the UCSC Genome Browser  
1015 Annotation Database.<sup>118</sup> We identified the nearest gene based on the priority of the variant  
1016 function (default ANNOVAR precedencies used) and the physical distance between the  
1017 respective variant and the gene. Moreover, we used ANNOVAR to predict transcript  
1018 consequences of non-synonymous exonic variants and added deleteriousness scores from CADD  
1019 (Combined Annotation Dependent Depletion),<sup>36</sup> DANN (Deep Neural Network for Annotating  
1020 pathogenicity),<sup>37</sup> and REVEL (Rare Exome Variant Ensemble Learner)<sup>38</sup> provided in dataset  
1021 dbnsfp35a (hg19).<sup>119</sup> We also added information on the cytogenetic band of each variant.

### 1022 **Gene nomination through functional annotation of credible variants**

1023 Credible variants were annotated using ANNOVAR (see section above),<sup>35</sup> and variant posterior  
1024 probabilities (see section 'credible sets of variants') were aggregated for each implicated gene.  
1025 Genes were ranked according to their aggregated posterior probabilities and nominated for gene  
1026 prioritization. Genes implicated by non-synonymous exonic variations were separately  
1027 nominated for gene prioritization. Implicated genes were ranked based on the CADD phred-  
1028 scaled scores of the non-synonymous exonic variant. If a gene was implicated by multiple non-  
1029 synonymous variants, the top CADD phred-scaled score was used.

### 1030 **Gene nomination through Summary-data-based Mendelian Randomization**

1031 We used summary-data-based Mendelian Randomization implemented in SMR v.1.03<sup>40,41</sup> to test  
1032 if the effect of an identified variant is potentially mediated by expression or splicing of a certain  
1033 gene. The SMR software provides an integrative approach that combines GWAS summary  
1034 statistics of complex phenotypes with information of omics resources to help prioritize gene  
1035 targets and regulatory elements. It adopts the Mendelian Randomization (MR) strategy by using

1036 a genetic instrument ( $z$ ) to test for pleiotropic association between gene regulation (exposure;  $x$ )  
1037 and a trait of interest (outcome;  $y$ ). The MR effect of gene regulation on a trait ( $\beta_{xy}$ ) is calculated  
1038 as two-step least squares estimate and defined as the ratio of the instrument effect on the  
1039 outcome ( $\beta_{zy}$ ) and that on the exposure ( $\beta_{zx}$ ), i.e.,  $\beta_{xy} = \beta_{zy}/\beta_{zx}$ . The term ‘pleiotropy’ is preferred  
1040 over ‘causality’ in this context, since SMR is based on a single genetic instrument and is unable  
1041 to distinguish between (horizontal) pleiotropy and causality (vertical pleiotropy). The SMR  
1042 software features the heterogeneity in dependent instruments (HEIDI) method, which uses  
1043 multiple instruments in the regulatory region to distinguish pleiotropy from linkage (i.e.,  
1044 transcript and phenotype are not associated because of a shared causal variant but due to two  
1045 or more distinct causal variants in linkage). We employed SMR with the BrainMeta v2 cis-eQTL  
1046 (gene expression) and cis-sQTL (gene splicing) summary statistics derived from RNA-sequencing  
1047 data of 2,865 brain cortex samples from 2,443 unrelated individuals of European ancestry.<sup>42</sup> Our  
1048 GWAS variants were successfully mapped to 16,375 eQTL and 58,941 sQTL probes. We only  
1049 considered results with  $FDR < 0.05$ ,  $p_{HEIDI} > 0.01$ , and those associations that could be assigned  
1050 to genome-wide significant loci from our discovery GWAS. We used the clumping procedure  
1051 implemented in PLINK v1.90b6.8 to assign significant SMR associations to discovered index  
1052 variations with a window-size of 3,000 kbp and  $R^2$  of 0.80. Genes implicated by eQTL and sQTL  
1053 SMR were separately nominated for gene prioritization and ranked according to SMR p-value.

#### 1054 **Gene nomination through GTEx eQTL lookup**

1055 Index variations and their genome-wide significant neighbors in strong linkage disequilibrium  
1056 ( $R^2 > 0.8$ ) were mapped to single-tissue and multi-tissue cis-QTLs cataloged in the Genotype-  
1057 Tissue Expression (GTEx) V8 database.<sup>120</sup> Significant variant-gene pairs for 49 tissues were  
1058 obtained using the prefiltered file provided by GTEx (GTEx\_Analysis\_v8\_eQTL.tar).  
1059 Multi-tissue QTLs were obtained using the METASOFT results for all 49 tissues  
1060 (GTEx\_Analysis\_v8.metasoft.txt.gz). Significant multi-tissue cis-QTLs were defined as  
1061 variant-gene associations with data available for at least 10 tissues and with an m-value  $\geq 0.9$   
1062 (i.e., the posterior probability that the effect exists) in at least 50% of the available tissues. Of  
1063 the remaining multi-tissue QTLs, a small fraction did not show convincing meta-analytic  
1064 p-values (across tissues) derived from the Han and Eskin's Random Effects Model (RE2). We  
1065 thus set an inclusion criterion of RE2  $p < 5E-8$  (met by 99.9% of remaining entries), which  
1066 resulted in a final number of 4,420,841 multi-tissue QTLs. Mapping our genome-wide significant  
1067 variants to single- and multi-tissue QTLs was carried out using the GTEx hg19 liftover variant  
1068 IDs. If multiple variants per discovered locus were associated with the expression of the same  
1069 gene in the same tissue (single-tissue QTL mapping) or associated with the expression of the  
1070 same gene across tissues (multi-tissue QTL mapping), respectively, we decided to only report  
1071 QTL results of the variant that is in strongest LD to the index variation of the discovered locus.

1072 We used the Bioconductor package `biomaRt`<sup>121</sup> to convert Ensemble gene IDs to HGNC gene  
1073 IDs and symbols. Genes implicated by GTEx single-tissue and multi-tissue eQTLs were  
1074 separately nominated for gene prioritization and ranked according to the number of significant  
1075 associations across tissues.

### 1076 **Gene nomination through Polygenic Priority Scores**

1077 We calculated polygenic priority scores using PoPS,<sup>43</sup> a similarity-based gene prioritization  
1078 method designed to pinpoint causal genes in significant GWAS loci. PoPS is applied on gene-  
1079 based results derived from MAGMA, and uses the full polygenic signal (including signals beneath  
1080 genome-wide significance) to identify the most likely causal genes. PoPS incorporates data from  
1081 a variety of sources, including 73 publicly available single-cell RNA sequencing datasets, curated  
1082 biological pathways, and protein-protein interaction (PPI) networks. In total, more than 57,000  
1083 features are used to prioritize genes. We used the same PoPS feature map and same MAGMA  
1084 gene annotation file as employed in the original work (downloaded from  
1085 <https://www.finucanelab.org/data>).<sup>43</sup> We applied MAGMA v.1.10 on our GWAS summary  
1086 statistics using the SNP-wise mean gene analysis with linkage information derived from the  
1087 discovery dataset (32,634 white-British ancestry individuals). For each index variant identified  
1088 through conditional analyses, we nominated up to three genes with the highest PoPS scores for  
1089 gene prioritization. Only genes located within 500 kb of the index variant and showing positive  
1090 scores were considered.

### 1091 **Gene prioritization**

1092 Genes considered for gene prioritization were nominated based on seven categories: 1) genes  
1093 implicated by functional annotation of credible variants (ranked by cumulative variant posterior  
1094 probabilities), 2) genes implicated by transcript consequences of non-synonymous exonic credible  
1095 variants (ranked by highest CADD deleteriousness score), 3) genes implicated by SMR eQTLs  
1096 (ranked by p-value), 4) genes implicated by SMR sQTLs (ranked by p-value), 5) genes  
1097 implicated by GTEx single-tissue eQTLs (ranked by number of significant associations across  
1098 tissues), 6) genes implicated by GTEx multi-tissue eQTLs (ranked by number of significant  
1099 associations across tissues), 7) genes implicated by PoPS (ranked by score). For each nominated  
1100 gene, we calculated a priority score as described below.

1101 Let  $i$  represent a specific gene, and  $j$  denote the index of the gene nomination analysis conducted.  
1102 The priority score ( $P_i$ ) for gene  $i$  is computed by considering both the cumulative posterior  
1103 probability ( $C_i$ ) obtained from the first gene nomination category and the ranks of the gene ( $R_{ij}$ )  
1104 across the six additional nomination categories ( $j \in [1,6]$ ). The formula is expressed as:

$$P_i = C_i + \sum_{j=1}^6 \frac{(n_j + 1 - R_{ij})}{\frac{n_j(n_j + 1)}{2}} = C_i + \sum_{j=1}^6 \frac{2(n_j + 1 - R_{ij})}{n_j(n_j + 1)}$$

1106 where...

1107  $P_i$  denotes the priority score for gene  $i$

1108  $C_i$  represents the cumulative posterior probability for gene  $i$

1109  $n_j$  denotes the number of genes ranked in nomination category  $j$

1110  $n_j + 1 - R_{ij}$  expresses the relative position of gene  $i$  in the ranking. For example, if gene  $i$

1111 holds the top position ( $R_{ij} = 1$ ), this term evaluates to  $n_j$ , reflecting the

1112 maximum possible contribution.

1113  $\frac{n_j(n_j+1)}{2}$  calculates the total number of fractions (1 point per category in total) that can

1114 be assigned to all genes within a nomination category

1115 We designate the gene with the highest priority score per locus as the prioritized gene, indicating  
1116 that it holds the highest probability of being causal.

### 1117 **GWAS catalog search**

1118 All index variations from the SNP-level analyses and their genome-wide significant neighbors in  
1119 strong linkage disequilibrium ( $R^2 > 0.8$ ) were selected for an NHGRI (National Human Genome  
1120 Research Institute) GWAS catalog search. Index variations were identified through conditional  
1121 analysis (see section ‘Conditional analysis’). Genome-wide significant neighbors in strong linkage  
1122 disequilibrium were identified by carrying out a  $p$ -value informed clumping procedure with  
1123  $R^2 > 0.8$  and 3,000 kb window-size implemented in PLINK v1.90b6.8. We used the GWAS  
1124 catalog released on December 21, 2021 (gwas\_catalog\_v1.0-associations\_e105\_r2021-12-21.tsv  
1125 received from <https://www.ebi.ac.uk/gwas/api/search/downloads/full>). We only considered  
1126 GWAS catalog entries that met genome-wide significance.

### 1127 **Gene-based analysis**

1128 Gene-based analysis were carried out using fastBAT as implemented in GCTA 1.93.1f.<sup>69</sup> Gene  
1129 coordinates were obtained from the RefSeq gene annotation file in GFF3 format (genome-build  
1130 GRCh37.p13; annotation release 105.20201022).<sup>117</sup> NCBI chromosome names were converted to  
1131 UCSC format. We selected genes of biotype ‘protein\_coding’ located on chromosomes 1-22, X,  
1132 Y, and MT. In the case of duplicate gene names, only the first entry was kept after sorting by  
1133 chromosome, gene symbol, start coordinate, and end coordinate. This resulted in 19,319  
1134 protein-coding genes, of which 18,583 were successfully mapped to SNPs and INDELs included  
1135 in GWAS analyses. We ran fastBAT with linkage information derived from the discovery dataset  
1136 (32,634 white-British ancestry individuals). The window around gene boundaries was set to 0 kb  
1137 to reduce dependencies between gene associations. Genes with  $FDR < 0.05$  (Benjamini &

1138 Hochberg) were regarded as significant after multiple testing correction. To identify independent  
1139 discoveries, we carried out a  $p$ -value informed clumping procedure with a conservative window-  
1140 size of 3,000 kbp. To identify distinct discoveries across the three BAG traits, we performed a  
1141 2nd-level clumping procedure based on the top  $p$ -value of each gene across traits, again with  
1142 3,000 kbp window-size.

### 1143 **Pathway analyses**

1144 Gene Ontology (GO) pathway analyses were conducted using R package GOfuncR 1.14.0 with  
1145 Bioconductor database Homo.sapiens v1.3.1 build upon GO.db v3.14.0.<sup>71,72,122,123</sup> The GO  
1146 annotation knowledgebase is a curated collection of biological terms and their relationships in  
1147 order to categorize genes and their products based on their involvement in ‘molecular processes’,  
1148 the ‘cellular components’ where they perform actions, and the higher-order ‘biological processes’  
1149 they contribute to. We used a set of selected genes (genes prioritized through positional and  
1150 transcription-based colocalization strategies and those with gene-based FDR < 0.05) to perform  
1151 overrepresentation analyses of GO terms using the hypergeometric test implemented in  
1152 GOfuncR. The total count of genes included in overrepresentation tests was 201, 339, and 303  
1153 for grey matter, white matter, and combined grey and white matter brain age, respectively. We  
1154 also conducted gene set enrichment analyses (GSEA) based on the complete gene-based result  
1155 table to test for lower-than-expected ranks ( $p$ -values) of gene sets using the Wilcoxon rank-sum  
1156 test implemented in GOfuncR. By default, GOfuncR calculates family-wise error rates for terms  
1157 in each of the three GO aspects based on random permutations. To reduce the chance of false  
1158 discoveries, we integrated these permutation-based results to calculate family-wise error rates  
1159 across the three GO aspects. In addition, we refined results with FWER < 0.05 by decorrelating  
1160 GO terms and restricting results to the most specific terms using the implemented elim  
1161 algorithm.<sup>124</sup> For result evaluation and interpretation, we determined the number of distinct loci  
1162 of genes that contribute to a GO term (using a 3,000 kbp clumping window) in order to account  
1163 for spatial clustering of genes and potential gene result dependencies.

### 1164 **Polygenic score analysis in replication sample**

1165 We used PRSice-2 to calculate polygenic scores (PGS) for BAG in the well-powered UKB  
1166 European ancestry replication sample.<sup>125</sup> Polygenic scores were computed based on variants  
1167 reaching ten pre-defined discovery  $p$  thresholds: 1.00, 0.50, 0.20, 0.10, 0.05, 0.01, 1.0e-03, 1.0e-04,  
1168 1.0e-06, 5.0e-08.<sup>82,126</sup> Variants with replication MAF < 0.01 were discarded. Variants were  
1169 clumped with  $R^2 < 0.1$  and 500 kbp window-size. Associations between the ten resulting PGS  
1170 and BAG were calculated as partial correlations using sex, age, age<sup>2</sup>, scanner site, total  
1171 intracranial volume, genotyping array, and the first 10 genetic principal components serving as  
1172 covariates.

1173 **Genetic correlations**

1174 We carried out bivariate LD score regression<sup>79</sup> to compute pair-wise genetic correlations both  
1175 among BAG traits and between BAG traits and other complex traits. Bivariate LD score  
1176 regression was run with 38 selected traits, which have frequently been used in similar  
1177 investigations and cover a broad range of mental and physical health domains.<sup>80-82</sup> In addition,  
1178 we calculated genetic correlations with a set of 989 heritable UK biobank traits, whose GWAS  
1179 summary statistics have been made publicly available by Neale and colleagues (Zenodo:  
1180 <https://doi.org/10.5281/zenodo.7186871>). LD score regression analyses included HapMap3  
1181 variants after exclusion of variants in the MHC region (variant list downloaded from  
1182 [http://ldsc.broadinstitute.org/static/media/w\\_hm3.noMHC.snplist.zip](http://ldsc.broadinstitute.org/static/media/w_hm3.noMHC.snplist.zip)). Genetic correlations  
1183 with  $FDR < 0.05$  were regarded as significant after multiple testing correction.

1184 **Mendelian randomization**

1185 Evidence for potential causal associations between BAG and other complex traits was derived  
1186 using generalized summary-data-based Mendelian Randomization (GSMR) as implemented in  
1187 GCTA 1.93.1f.<sup>32,83</sup> The GSMR method uses multiple genetic variants as instruments ( $z$ ) to test  
1188 for causality between an exposure ( $x$ ) and outcome variable ( $y$ ). Instruments are near-  
1189 independent genetic variants (clumped with  $R^2 < 0.05$ ) associated with the exposure variable at  
1190 a genome-wide significance level. GSMR is designed for two-sample scenarios, that is, GWAS  
1191 summary-statistics of large independent studies are used to estimate the effects of the exposure  
1192 on the outcome ( $\beta_{xy}$ ) based on the effects of the instruments on the exposure ( $\beta_{zx}$ ) and the effects  
1193 of the instruments on the outcome ( $\beta_{zy}$ ). The ratio between  $\beta_{xy}$  and  $\beta_{zx}$  reveals the estimated  
1194 mediation effect, i.e.,  $\beta_{xy} = \beta_{zy}/\beta_{zx}$ , which is expected to be identical at each instrument under a  
1195 causal model. Estimates from multiple instruments are integrated in a generalized least-squares  
1196 approach. The use of multiple instruments enables to distinguish between causality, where the  
1197 effect of an instrument on the outcome is mediated by the exposure, and horizontal pleiotropy,  
1198 where the effect of an instrument on the outcome is exhibited through pathways other than the  
1199 exposure. GSMR tests for heterogeneity in dependent instruments (HEIDI) to remove outliers  
1200 based on the deviation of each instrument from the causal model. We used the default setting  
1201 of removing HEIDI-outliers with deviation  $p < 0.01$ . To facilitate effect size comparisons, we  
1202 standardized instrument effects on continuous exposure variables ( $\beta_{zx}$ ) based on z-statistic, allele  
1203 frequency and sample size. GSMR has been demonstrated in simulations to be more powerful  
1204 than inverse-variance-weighted MR (MR-IVW) and Egger regression (MR-Egger).<sup>83</sup> Other  
1205 empirical investigations have revealed qualitatively similar results between GSMR, MR-IVW,  
1206 and MR-Egger.<sup>82</sup> For GSMR analyses, we selected 11 risk factors based on the availability of  
1207 summary statistics from large-scale GWAS that did not include the UK Biobank cohort and  
1208 provided at least  $m = 30$  independent genome-wide significant variants as instruments (clumped

1209 with  $R^2 < 0.05$ ). Due to the limited number of genome-wide significant variants for BAG, we  
1210 only conducted unidirectional GSMR analyses with BAG serving as outcome variable.

### 1211 **Polygenicity**

1212 We conducted genetic effect-size distribution inferences implemented in R package  
1213 GENESIS v1.0<sup>127</sup> to estimate the number of underlying susceptibility variants for BAG under a  
1214 normal-mixture model of variant effects. Analyses of the benchmark traits neuroticism and  
1215 height were based on the publicly available GWAS summary statistics by Baselmans et al.<sup>87</sup> and  
1216 Allen et al.<sup>128</sup> Variants were filtered to 1.07 million common variants with  $MAF \geq 0.05$  included  
1217 in the HapMap3 panel after exclusion of the major histocompatibility complex (MHC) region.  
1218 SNPs with less than 0.67 times the 90th percentile of sample sizes and those with extremely  
1219 large effect sizes ( $z^2 > 80$ ) were removed. We fitted the GENESIS three-component model, which  
1220 assumes that 99% of the variant effects are null and the remaining 1% follow a mixture of two  
1221 normal distributions, allowing a fraction of the susceptibility SNPs to belong to a cluster with  
1222 larger effect sizes. We have chosen the three-component model (M3) over the simpler two-  
1223 component model (M2), because a) M3 has been shown to provide distinctly better fits for a  
1224 variety of complex traits, b) M3 has been shown to perform well even if the true data does not  
1225 conform the model assumptions, and c) M2 appears to exhibit a more pronounced bias towards  
1226 underestimating the number of susceptibility SNPs, particularly if model assumptions are not  
1227 met.<sup>89</sup> We used default settings for defining tagging SNPs and LD scores by using an LD cutoff  
1228 of 0.1 and LD window of 1 Mbp.